University of Nevada

Reno

Transport Model for the Adsorption of Selenium in Packed Bed and Batch Tests with Aluminum and Lanthanum Oxides

A thesis submitted in partial fulfillment of the requirements for the degree of

Master of Science in Metallurgical Engineering

by

Samuel A. Davis

Manoranjan Misra, Thesis Advisor

December 1995

The thesis of Samuel A. Davis is approved:

Marvin Mix

Thesis Advisor

Thos W Smith

Department Chair

Dean, Graduate School

University of Nevada

Reno

December 1995

Table of Contents

List of Figures

List of Tables

Abstract:

Lanthanum oxide, activated γ-alumina, and activated α-alumina were tested as adsorbents for Se(IV) oxy-anions in batch and packed bed tests. Batch tests showed that lanthanum oxide is the best adsorbent for selenium when compared at the same solids and selenium concentrations. The packed bed tests showed that activated α-alumina has a higher loading capacity than activated γ-alumina (59 mg Se(IV)/gr versus 37 mg Se(IV)/gr) and is eluted with greater efficiency. Also, activated α-alumina is less degradable compared to activated γ-alumina during packed bed adsorption and regeneration stages. Electrokinetic measurements proved that lanthanum oxide is the most electropositive of the adsorbents tested, which accounts for its ability to remove selenium to lower levels than the activated aluminas tested. The driving force for adsorption was shown to consist of three gradients (concentration, potential, and hydrated ionic size), by modeling the batch and packed bed test results with a transport model.

II. Introduction:

i. Problem Statement:

Selenium is a highly toxic chemical that finds its way into various ecosystems because of its presence in industrial wastewater. Some of the major industrial operations which produce selenium containing wastewater are coal mining, petroleum refining, copper producing, lead/zinc ore milling, and zinc smelting. Selenium concentrations in these toxic effluents vary between 10^{-3} ppm and 7 ppm, with most below 1 ppm.[1] Selenium is used in the electronics industry and for the manufacture of rectifiers, photoconductivity cells, glass, ceramics, paints, pigments, dyes, enamels and insecticides.[1,2]

Due to the high toxicity and occurrence of selenium, it is listed as a priority pollutant by the United States Environmental Protection Agency (EPA).[3] This legislation has prompted academia, industry, and government to search for the most efficient and cost effective selenium remediation technologies. Commercial selenium removal technologies that are presently available are either too expensive or do not remove selenium effectively, especially at concentrations below 1 ppm.[4] Thus, with the financial support of the United States Bureau of Mines (USBM), Generic Center for Waste Treatment and Recovery (Grant # G1145232) and ENCYCLE/Texas, the University of Nevada, Reno, has investigated the use of various activated alumina (Al_2O_3), lanthanum oxide (La_2O_3), and mixed alumina/lanthanum oxides as adsorbents for remediation of selenium contaminated wastewater. Experimental efforts presented here include bench

scale tests in batch and packed bed systems and electrokinetic measurements. The goal of this work was to contribute to the development of a continuous, cyclic packed bed process for selenium removal and recovery utilizing the optimum combination of activated Al_2O_3 and La_2O_3.

ii. Toxicity:

1. Selenium:

Selenium is a cumulative toxic substance which causes a health hazard when present in food or water. However, at very low levels it is an essential nutrient for animals.[2] Selenium at concentrations required nutritionally is incorporated into specific functional proteins. At higher concentrations it is incorporated into molecules normally served by sulfur. Selenium analogs are often less stable than sulfur compounds, and this liability may be the basis for toxicity. The primary deposition sites for selenium in the body are the liver, kidney, spleen, and middle and lower sections of the small intestine, followed by the heart, lungs, brain, and muscle.[5]

At concentrations of 0.1 to 0.2 mg Se/Kg body weight, selenium is definitely toxic to humans. The toxic effects of selenium to humans can be mutagenic, teratagenic, comatosis, and respiratory failure. Toxic effects to humans due to overexposure of selenium may include loss of fingernails and "blind staggers." Blind staggers is the name applied to an acute form of selenium disease experienced by cattle. Though the animal is not blind and may not stagger, there is some impairment of vision, difficulty in judging near objects, and a tendency to wander. Paralysis and evidence of abdominal pain occur

in the final states of the disease; and death is due to respiratory failure. Alkali disease is a more chronic form of selenium poisoning of livestock than blind staggers.[5]

Selenium deficiencies such as "white muscle disease" also occur in livestock with equally debilitating results. Thus, it is clearer to see why selenium has beneficial nutritional effects for humans at very low levels. The Food and Drug Board of the National Research Council recommends that for adults a safe level of selenium intake is 50 to 200 μg/day. Most of this is obtained from vegetables, which accumulate selenium in the soil.[5]

2. Rare Earths:

The rare earths include the elements with atomic numbers 57 through 63, beginning with lanthanum, the lightest of the rare earths. Lanthanum is obtained from bastnasite, monazite, and xenotime ores. The toxicity of the rare earths falls into two categories: Nonradioactive and radioactive.[6]

The nonradioactive toxicity of rare earths is dependent upon the chemical form, its route of administration, and the individual rare earth. Overall, the rare earths are considered slightly toxic. Orally administered lanthanides are poorly absorbed by the gastrointestinal tract and have very low toxicity. When administered at levels as high as 1 to 10 grams of lanthanide oxides and lanthanide sulfates per Kg of body weight, the compounds were not lethal to small vertebrates. However, chronic exposures to lanthanide dust can lead to rare earth pneumoconiosis.[6]

The radioactive toxicity of rare earths is only encountered with neodymium, samarium, gadolinium, and lutetium, which have naturally occurring radioactive isotopes. The risk of toxicity from these natural isotopes is very low due to their extremely long half-lives and low radioactivity levels. However, rare earths often exist in ore and concentrates in association with other elements that have vastly different properties, including varying toxicities and radioactive emissions (i.e. uranium and thorium).[6] Thus, when purchasing lanthanum oxide, the degree of purity as well as the type of impurities is an important safety factor to consider. For instance, the La_2O_3 used in the experiments in this thesis contained about 100 ppm neodymium (III) oxide and 50 ppm lead (II) oxide.[7]

Therefore, La_2O_3 is a potentially hazardous compound that is considered non-toxic and has no threshold limit value (TLV) or carcinogenic potential. The possible acute effects of overexposure to La_2O_3 are irritation to the lungs and eyes. Chronic effects associated with La_2O_3 are that long term inhalation may damage lungs and that rare earth oxides (REO's), in general, may cause delayed blood clotting, leading to hemorrhages. The harmful effects of swallowing La_2O_3 are unknown, but are considered acute.[7]

3. Alumina:

Activated γ-Al_2O_3 can cause fibrosis of the lungs, if inhaled at high concentrations for long or short periods, or at low concentrations for long periods. Overall, alumina is a low health risk by inhalation and should be treated as a nuisance dust as specified by the American Conference of Governmental Industrial Hygienists.[8] However, Al_2O_3 may

cause irritation to the eyes and upper respiratory tract due to its desiccant properties. The TLV and Permissible Exposure Level (PEL) for γ-Al_2O_3 are, respectively, 10 and 5 mg/m^3.[9]

iii. Regulations:

According to the Safe Water Drinking Act, the 1992 Maximum Contaminant Level (MCL) for groundwater and the interim primary drinking water standard for selenium is 10 ppb.[10] The EPA hazardous waste number for selenium is D010.[11] The EPA Best Available Technologies (BAT's) for selenium are activated alumina; coagulation/filtration (Se(IV) only); lime softening; reverse osmosis; and electrodialysis.[10]

Although the EPA sets guidelines for MCL's and safe drinking water, state and city governments often set their own standards for industrial and municipal wastewater. For instance, the selenium discharge limit to the Reno, Nevada, sewer system from our lab is 40 ppb. More importantly, state agencies set wastewater selenium effluent limitations for various industries, which are a function of the amount of wastewater produced; location of wastewater discharge; etc. For example, one California refinery is allowed to discharge up to 50 ppb selenium into the Pacific Ocean, whereas ENCYCLE/Texas, Corpus Christie, Texas, is permitted to discharge 500 ppb selenium into the Gulf of Mexico from their wastewater treatment facility.[4] Newmont Gold Company, in Carlin, Nevada, must discharge wastewater with less than 1 ppb selenium.

Common analytical methods for selenium detection include Atomic Absorption (AA) and Inductively Coupled Plasma (ICP) Spectroscopy. ICP is only accurate at concentrations below 500 ppb. For concentrations down to about 1 ppb, gaseous hydride generation, coupled with AA detection, is recommended. Alternatively, AA may be used with a graphite furnace.[11]

III. Previous Work:

i. UNR Research:

1. Adsorption of Synthetic Solutions:

Batch tests performed in this area were mainly for determining the adsorption capacity and kinetics of γ-Al_2O_3, α-Al_2O_3, and La_2O_3 for oxy-anions of selenium and arsenic at different concentrations and pH values. About 2 gr of the respective oxide adsorbent was placed in a 250 ml PYREX flask at a controlled temperature and stirring speed, and a known volume and concentration of selenium was added. Concentration was measured as a function of time for each initial pH.[12]

Conclusions made from this research were as follows: The major adsorbed selenium species is biselenite ($HSeO_3^-$); the adsorption efficiency is a function of pH and initial concentration; adsorption is only appreciable at a pH lower than the pH_{pzc}; adsorption increases with decreasing pH until the point where most of the Se(IV) exists as selenious acid (near pH = 2); activated γ-Al_2O_3 and La_2O_3 are the best adsorbents for selenium of the oxides tested; and La_2O_3 removes selenium most effectively of the oxides tested. Also the pH_{zpc} of activated γ-Al_2O_3 and La_2O_3, respectively, were found to be 9.2

and 10.2. From this, it was concluded that the high pH_{zpc} of La_2O_3 accounts for its greater affinity for selenium.[12]

2. Adsorption of Stripped and Biotreated Sour Water:

Batch adsorption experiments were performed on stripped sour water and biotreated sour water from a California petroleum refinery, using activated γ-Al_2O_3, activated α-Al_2O_3, and La_2O_3. The initial and final concentration was recorded for each adsorbent and wastewater. The results are given in Table I ($LA^{(T)}$ refers to a mixture of 10% La_2O_3 and 90% γ-Al_2O_3):[13]

Table I: Removal of selenium from stripped and biotreated sour water.

Biotreated Sour Water, Initial Selenium Concentration 0.238 ppm	
Adsorbent	**Total Se Concentration (ppm)**
activated α-Al_2O_3	0.100
activated γ-Al_2O_3	0.040
$LA^{(T)}$	0.036
Stripped Sour water, Initial Selenium Concentration 1.552 ppm	
Adsorbent	**Total Se Concentration (ppm)**
activated γ-Al_2O_3	1.051
$LA^{(T)}$	1.052
activated γ-Al_2O_3 (double mass than above)	0.939
$LA^{(T)}$ (double mass than above)	0.917

These results show that the adsorption process was only effective with the biotreated wastewater. This was mainly because the biotreated water was oxidized to selenite or biselenite. Furthermore, the pH of the biotreated water was between 6.5 and 8.5, which was lower than the stripped sour water pH range (refer to Table II).

Table II: Selenium-bearing refinery wastewater streams.[4]

Parameter	Stripped Sour Water	Final (biotreated) Effluent
flow rate (gpm)	100 - 1000	2000 - 5000
pH	6 - 12	6.5 - 8.5
temperature (C)	80 - 115	20 - 35
total selenium (ppb)	1000 - 5000	50 - 300
selenium species:		
selenide (%)	< 20	0
elemental selenium (%)	< 10	0
selenite (%)	< 5	10 - 95
selenate (%)	< 1	< 30
total sulfur (mg S/L)	50 - 200	300 - 800
sulfur as sulfate (%)	< 1	100
ammonia (mg N/L)	20 - 200	< 5
nitrate (mg N/L)	0	5 - 30
total dissolved solids (mg/L)	200 - 2000	2000 - 7000
total hardness (mg $CaCO_3$/L)	< 20	50 - 300
total alkalinity (mg $CaCO_3$/L)	< 20 - 1000	50 - 300
total organic carbon (mg/L)	500 - 10000	< 50
chemical oxygen demand (mg/L)	2000 - 30000	< 50
biochemical oxygen demand (mg/L)	500 - 10000	< 30
total suspended solids (mg/L)	50 - 200	< 30

ii. Industrial Process Water:

Research was conducted by ENCYCLE/Texas and the Paradise Peak mine near Gabbs, Nevada (which is now shut down and in the process of land reclamation), to determine the effectiveness of various alumina and lanthanum oxides for selenium removal. The results of these experiments were used to assist in developing a selenium removal process.

Batch adsorption tests conducted with ENCYCLE's process water showed that the best adsorbent for their problem was a mixture of α-Al_2O_3 (DD-6) and La_2O_3. This

was because this adsorbent combination removed selenium to below the detection limit and also lowered the arsenic concentration to the lowest level of all the oxides tested. Also, they found that the high sodium level of 8360 ppm did not compete for adsorption with selenium or arsenic, as the sodium concentration remained essentially unchanged.[4]

Workers at Paradise Peak conducted column tests with several commercial brands of activated α-Al_2O_3 to find the best adsorbent for selenium removal. Of the adsorbents tested, DD-6 had the highest loading (at 0.43 mg Se/gr DD-6). In their experimental method, after the column became saturated with selenium, it was eluted from the column with 0.1 N sulfuric acid, with about 90% recovery. The other aluminas tested had lower selenium loadings and similar elution recoveries. From the limited information given, it appears that the entire operating cycle consisted of wastewater treatment and elution with sulfuric acid.[4]

iii. EPA Column Tests:

In these experiments, fresh activated α-alumina was prepared for use and then regenerated after the adsorbent became loaded. Fresh adsorbent was prepared by the following method:[8]

1. 1% NaOH rinse for 50 minutes.
2. 5 minute D.I. water rinse.
3. 0.05 N HCl rinse for 10 minutes (for Se(IV)).
4. 0.05 N H_2SO_4 rinse for 10 minutes (for Se(VI)).
5. 2-4 D.I. rinses for 5 minutes each..

Loaded adsorbent was regenerated by the following scheme for tests with Se(IV):[8]

1. 5 bed volumes 0.5% NaOH at 0.5 gpm/ft^2, up.
2. 5 bed volumes D.I. water at 0.5 gpm/ft^2, up.
3. 6 bed volumes 0.05 N HCl at 1 gpm/ft^2, up.
4. 5 bed volumes D.I. water at 1 gpm/ft^2, up.

Upflow was chosen because it facilitated rapid testing. Upflow regeneration by NaOH was recommended, but it was suggested that the remaining steps should be downflow in a full-scale removal facility. Using the above steps for regeneration, the following dissolution of activated α-alumina was recorded:[8]

1. NaOH: 0.9% per regeneration.
2. H_2SO_4 (or HCl): 0.08% per regeneration.

The flow rate of the NaOH regeneration solution was one of the most important operating parameters for tests with Se(IV). For column tests with Se(VI), the rate of regeneration was not as important of a parameter, and a smaller dose of NaOH was used. This was due to the low selectivity of Se(VI).[8]

iv. Chemistry of Selenium:

The chemistry of selenium is quite complex because the stability of a given ion depends on the pH and Eh. Figures 1 through 3 show the speciation of selenium at various oxidation states. At the most oxidized conditions in acidic water, selenium exists as the conjugate base of the strong acid, selenic acid (H_2SeO_4), which dissociates in water by losing one of its protons. Selenic acid is comparable to sulfuric acid in strength and chemical behavior. Selenious acid (H_2SeO_3) is a weak acid. In the pH range of 6.5 to 8.5, and under a normal Eh range of about -0.2 to 1.0, the most common forms of

Figure 1: Distribution of selenium (VI) as a function of pH.
– Se(VI) concentration 0.5 ppm.

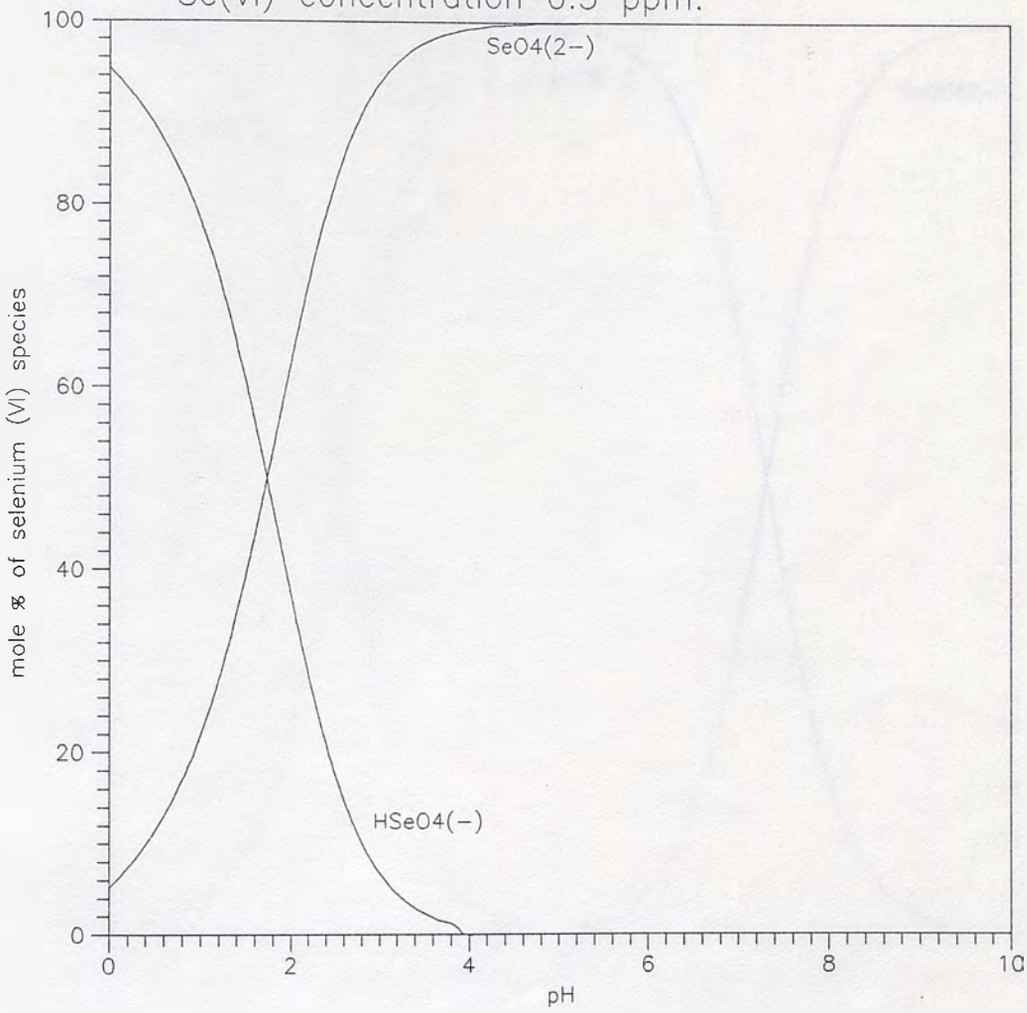

Figure 2: Distribution of selenium (IV) as a function of pH.
– Se(IV) concentration 0.5 ppm.

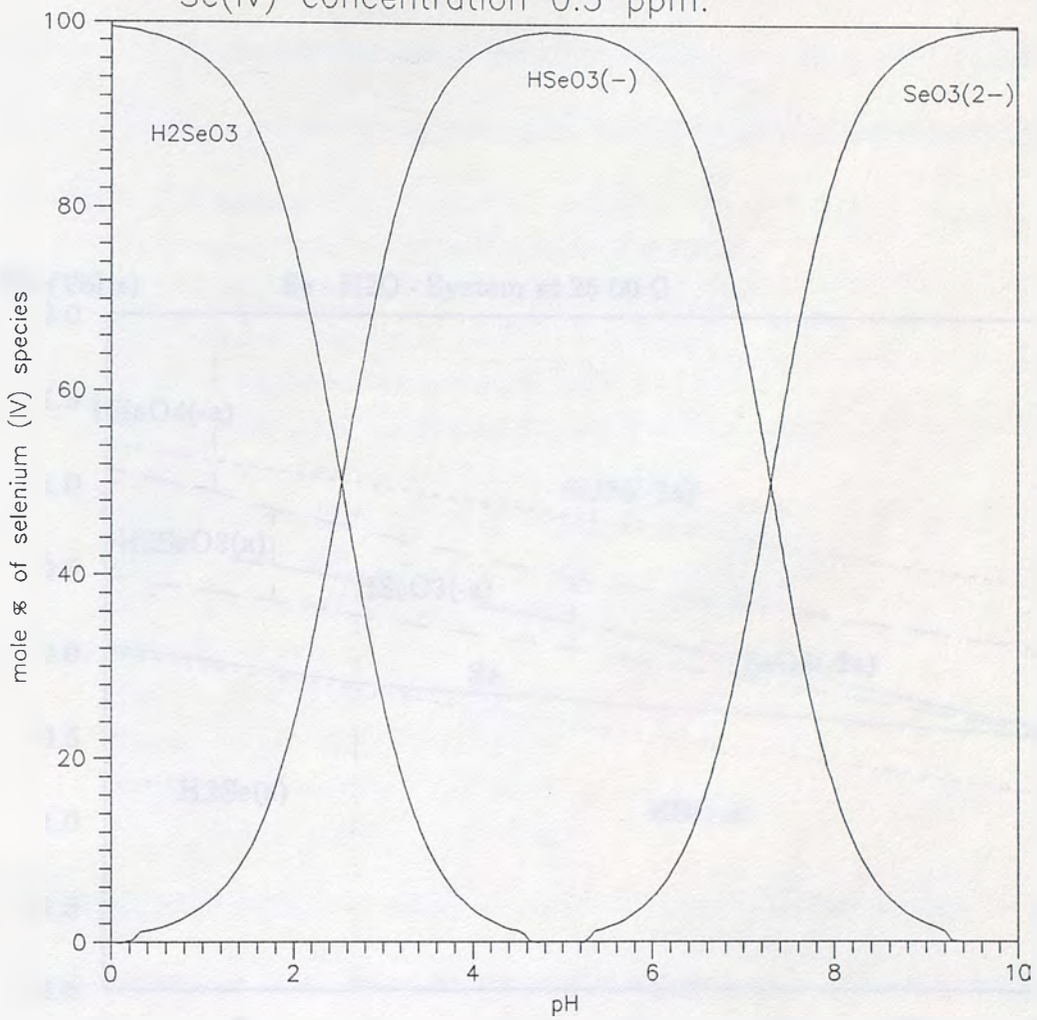

Figure 3: Pourbaix diagram for selenium.
- Selenium concentration 0.5 ppm.
- Ionic strength 0.01.

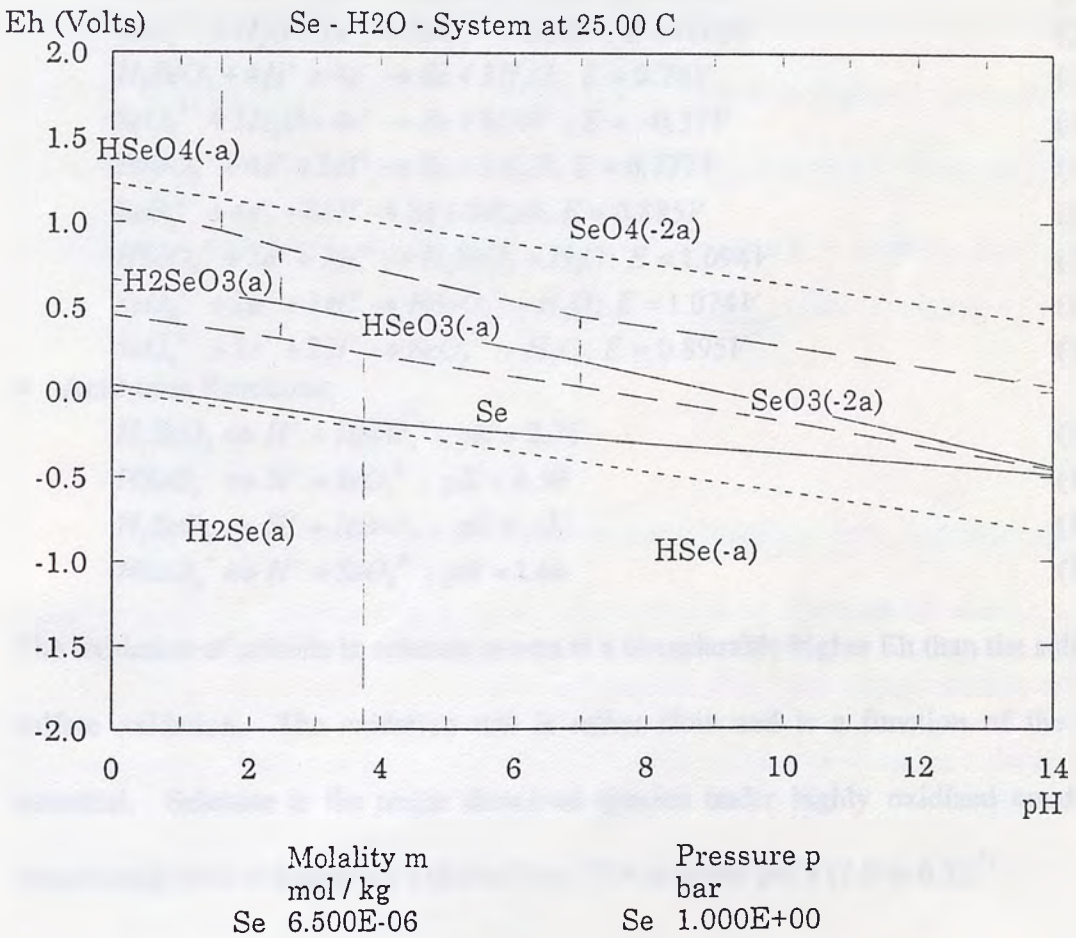

selenium are biselenite and selenate ($HSeO_3^-$ and SeO_4^{2-}, respectively). In general, selenium in aqueous solutions, within the solubility limits of water, exists in the +4 or +6 valance state. At highly acidic and oxidized conditions, selenic and selenious acid are stable. At basic conditions, selenate and selenite are predominant. In between, biselenite and biselenate are present. Selenium can also exist as part of a number of organic compounds, but the concentration of these forms of selenium are usually negligible. The half-cell reactions and acid-base reactions for Se (IV) and Se (VI) are given below:[8,12]

- Half-cell Reactions:

$$SeO_4^{2-} + 4H^+ + 2e^- \rightarrow H_2SeO_3 + H_2O\ ;\ E = 1.15V \quad (1)$$
$$SeO_4^{2-} + H_2O + 2e^- \rightarrow SeO_3^{2-} + 2OH^-\ ;\ E = 0.05V \quad (2)$$
$$H_2SeO_3 + 4H^+ + 4e^- \rightarrow Se + 3H_2O\ ;\ E = 0.74V \quad (3)$$
$$SeO_3^{2-} + 3H_2O + 4e^- \rightarrow Se + 6OH^-\ ;\ E = -0.37V \quad (4)$$
$$HSeO_3^- + 4e^- + 5H^+ \rightarrow Se + 3H_2O;\ E = 0.777V \quad (5)$$
$$SeO_3^{2-} + 4e^- + 6H^+ \rightarrow Se + 3H_2O;\ E = 0.885V \quad (6)$$
$$HSeO_4^- + 2e^- + 3H^+ \rightarrow H_2SeO_3 + H_2O;\ E = 1.094V \quad (7)$$
$$SeO_4^{2-} + 2e^- + 3H^+ \rightarrow HSeO_3^- + H_2O;\ E = 1.074V \quad (8)$$
$$SeO_4^{2-} + 2e^- + 2H^+ \rightarrow SeO_3^{2-} + H_2O;\ E = 0.895V \quad (9)$$

- Acid-base Reactions:

$$H_2SeO_3 \Leftrightarrow H^+ + HSeO_3^-\ ;\ pK = 2.75 \quad (10)$$
$$HSeO_3^- \Leftrightarrow H^+ + SeO_3^{2-}\ ;\ pK = 8.50 \quad (11)$$
$$H_2SeO_4 \rightarrow H^+ + HSeO_4^-\ ;\ pK = -3 \quad (12)$$
$$HSeO_4^- \Leftrightarrow H^+ + SeO_4^{2-}\ ;\ pK = 1.66 \quad (13)$$

The oxidation of selenite to selenate occurs at a considerably higher Eh than the sulfide to sulfate oxidation. The oxidation rate is rather slow and is a function of the redox potential. Selenate is the major dissolved species under highly oxidized conditions, constituting 95% at higher pH's (8.5 to 9) to 75% at lower pH's (7.5 to 6.5).[12]

The anions and acids of Se(VI) and Se(IV) occur as tetrahedral and pyramidal species, respectively. The symmetries c_s and c_{3v} (trigonal-pyramidal) were assigned to the anions $HSeO_3^-$ and SeO_3^{2-}, respectively. Raman spectra of H_2SeO_4, $HSeO_4^-$ and SeO_4^{2-} show vibrational frequencies assigned according to the tetrahedral symmetries c_{2v}, c_3, and T_d, respectively.[14]

v. Adsorption Mechanism:

Numerous studies have been conducted to determine the mechanism of adsorption of oxyanions of selenium at the oxide-water interface of activated Al_2O_3, Goethite, and amorphous iron oxyhydroxide. In all cases, the surface is assumed to be composed of amphoteric hydroxyl groups which can be positive, neutral or negative, depending on the pH and pH_{zpc} of the metal oxide and the supporting electrolyte composition. The equilibria of the surface hydroxyls is expressed below (S = surface; H_s^+ = surface hydrogen ion; and $K_{a1\text{-}a2}^{int}$ = intrinsic equilibrium constants):[15,16]

$$SOH_2^+ \xleftrightarrow{K_{a1}^{int}} SOH + H_s^+ \qquad (14)$$

$$SOH \xleftrightarrow{K_{a2}^{int}} SO^- + H_s^+ \qquad (15)$$

There are three general mechanisms for adsorption with activated Al_2O_3 in aqueous systems: chemisorption by covalent attachment, electrostatic charge, and ion exchange. In deriving the chemisorption mechanism, the hydroxylated surface is treated as a polymeric oxyacid or base. The specific reactions that can occur for a metal ion are given by (where M^{z+} is a metal cation):[17]

$$SOH + M^{z+} \xleftrightarrow{K_1} SOM^{(z-1)} + H^+ \qquad (16)$$

$$2(SOH) + M^{z+} \xleftrightarrow{K_2} SO - M^{(z-2)} - O - S + 2H^+ \quad (17)$$

Some examples of metallic cation binding via chemisorption are given by the stability constants in Table III:[17]

Table III: Representative stability constants for surface metal complexes on a transition activated γ-Al_2O_3.[17]

Metal	log (K_1)	log (K_2)	I
Ca^{2+}	-6.1		0.1 M $NaNO_3$
Mg^{2+}	-5.4		0.1 M $NaNO_3$
Ba^{2+}	-6.6		0.1 M $NaNO_3$
Pb^{2+}	-2.2	-8.1	0.1 M $NaClO_4$
Cu^{2+}	-2.1	-7.0	0.1 M $NaClO_4$

In cases where adsorbing metals are bound even against electrostatic repulsion, the chemical binding energy must predominate.[17]

Coordination of selenium as selenate is an example of anion chemisorption with ligand exchange:

$$SOH + SeO_4^{2-} \rightarrow S - SeO_3^- + OH^- \quad (18)$$

For protonated anions, such as selenite, surface deprotonation of the ligand may occur with exchange:[17]

$$SOH + SeO_2(OH)^- \rightarrow SO - SeO_2H + OH^- \rightarrow S - SeO_2^- + H_2O \quad (19)$$

The electrostatic charge mechanism is a result of surface protonation. Since all activated aluminas are highly electropositive below the pH_{zpc}, the surface can attract negative oxyanions of selenium by coulombic forces.[17]

The third mechanism for adsorption with activated aluminas is ion exchange. The primary exchange reactions for anions (X^-) and cations (M^{z+}) are given by:[17]

$$SO^- + M^{z+} \longleftrightarrow SO - M^{(z-1)} \quad (20)$$

$$SOH_2^+ + X^- \longleftrightarrow SOH_2^+ - X^- \quad (21)$$

Exchange is favored for aqueous anions at low pH's and cations at high pH's.[17]

Mechanisms assessed for other mineral surfaces may also apply to activated Al_2O_3 and La_2O_3 to some extent, since the surfaces are all similar. Several workers have characterized the mechanism of adsorption by the type of complex that forms. In the case of non-specific adsorption (ion exchange mechanism), the adsorbed anion will form an outer-sphere (OS) complex with the surface hydroxyl, and maintain its primary hydration sheath. For specific adsorption, an inner-sphere (IS) complex will be formed. Examples of these are given below for selenite and selenate:[18]

- Selenite:

$SOH_2^+ + HSeO_3^- \longleftrightarrow SOH_2^+ - HSeO_3^-$	OS	(22)
$SOH_2^+ + SeO_3^{2-} \longleftrightarrow SOH_2^+ - SeO_3^{2-}$	OS	(23)
$SOH_2^+ + HSeO_3^- \longleftrightarrow S(HSeO_3) + H_2O$	IS	(24)
$SOH_2^+ + SeO_3^{2-} \longleftrightarrow S(SeO_3^-) + H_2O$	IS	(25)

- Selenate:

$SOH_2^+ + SeO_4^{2-} \longleftrightarrow SOH_2^+ - SeO_4^{2-}$	OS	(26)
$SOH_2^+ + SeO_4^{2-} \longleftrightarrow S(SeO_4^{2-}) + H_2O$	IS	(27)

Other possible reactions include IS and OS, bidentate complexes. It was found, by EXAFS spectroscopy on Fe oxides, that selenite and arsenate form binuclear, bidendate and mononuclear, monodentate IS complexes and selenate forms mainly OS complexes.[18]

Thus, there are several competing mechanisms responsible for adsorption of oxyanions of selenium at the oxide-water interface.

vi. Mathematical Modeling:

Previous researchers who have developed adsorption models for metal oxides have used simplistic assumptions about the mechanism or have only considered steady-state conditions. Examples of these include the Triple Layer, Langmuir, Stern, Grahame, and Stern-Grahame models.[15,16,19,20] For instance, the Grahame model is limited for use with surface excesses less than monolayer coverage, and the Langmuir isotherm will not account for the formation of binuclear, bidentate, IS surface complexes, which are thought to occur when selenite and arsenate adsorb onto metal oxides.[18]

The most commonly used model for the adsorption process is "the method of second-order kinetics." This method assumes the following reaction between sorbate and sorbent:[21]

$$sorbate + sorbent \rightarrow sorbate - sorbent \tag{28}$$

By assuming a Langmuir-type equilibrium, the rate of adsorption for this mechanism is given by:[21]

$$\frac{dq}{dt} = k\left[C\left(Q^{\circ} - q\right) - \frac{q}{b}\right] \tag{29}$$

Where q is the concentration of the sorbate on the sorbent and C is the concentration of the sorbate in the bulk solution. Q° is the ultimate monolayer capacity of sorbent for the sorbate, and b is the Langmuir equilibrium constant, relating to the free energy of adsorption. At steady state, equation (29) reduces to the Langmuir isotherm equation.[21]

For a batch system, the following relationships may be used with equation (29) to reduce the system to a non-linear differential equation with one dependent variable and time as the independent variable; where C_s is the solids concentration and C_0 is the initial bulk solution concentration:

$$q = \frac{(C_0 - C)}{C_s} \tag{30}$$

$$\frac{dq}{dt} = -\frac{1}{C_s}\frac{dC}{dt} \tag{31}$$

For a packed bed system, equation (29) (with time replaced by volume and volumetric flowrate) may be combined with equation (73) and solved numerically for concentration and loading as a function of volume treated and bed length. This method is outlined in *Perry's Chemical Engineers' Handbook, 6th Ed.* The shortcomings of the second-order method are that it is not very accurate when used with multicomponent systems, and the equations cannot be made fully predictive, as they do not reveal the effects of pH; pH_{zpc}; diffusion coefficient; ionic charge and size; specific surface area; Reynolds number; etc.

vii. Alternative Technologies for Selenium Removal:

1. Patented Selenium Removal Techniques:

Several techniques for removing selenium from water, besides ion exchange, distillation, and reverse osmosis, have been demonstrated to work with high efficiencies. The technique found in patent 3,933,635 gave 60% to 98% reduction of selenious acid when elemental zinc was added to a solution with a pH between 1 and 4, at temperatures

between 25 and 85 °C. The reaction took 1 to 10 minutes. A 2-stage cocurrent reactor was used. Aluminum and aluminum can scrap also gave good removal efficiencies.[22]

The process found in patent 4,405,464 gave 75% to 99% reduction of Se (VI) to Se (IV) when elemental iron was added to a solution. The Se (IV) was precipitated with $Fe(OH)_2$.[23]

A third process found in patent 4,519,913 involved using a porous matrix populated with bacteria that biochemically reduced aqueous selenium species to elemental selenium under anaerobic conditions. The process was slow, but efficient, using the bacteria genus clostridium. The progress of the reaction was monitored visually because elemental selenium is red and the bacteria changed to this color when the reduction reaction was complete.[24]

The pitfalls of the zinc and iron processes are that these elements are expensive compared to activated Al_2O_3, and both processes require precipitation after the reduction reactions. The process involving bacteria is less costly than the others, but the rate of the reaction is too slow to permit industrial scale use.[22,23,24]

2. Ion Exchange:

Recently, a specialty chelating polymer, with immobilized Cu(II) at the sorption sites, was found to have high selectivity for selenate and arsenate in the presence of sulfate. In these experiments, an acrylic column was loaded with DOW 2N ion exchange resin (XFS 43084, a chelating exchanger, with a macroporous polystyrene matrix) and saturated with Cu(II) ions. The ratio of column diameter to exchanger bead diameter was

approximately 20, to minimize channeling. The Cu(II) saturated resin was used to adsorb oxyanions of selenium from solution with the following selectivity:

$$SeO_4^{2-} > SO_4^{2-} > SeO_3^{2-} > NO_3^- > Cl^-$$

This procedure would be useful for industrial wastewater with high selenate and sulfate concentrations.[3]

3. SORBPLUS by ALCOA:

$LA^{(T)}$ will be competitive with SORBPLUS, a mixed-metal oxide developed by ALCOA as an adsorbent for anions and cations from aqueous streams. SORBPLUS is a magnesium oxide-aluminum oxide (hydrotalcite-like) adsorbent. Since lanthanum oxide is more electropositive than magnesium oxide, $LA^{(T)}$ is better suited to remove negative ions, such as oxyanions of selenium and arsenic, than SORBPLUS, particularly at low concentrations. The main advantage of using SORBPLUS, is that it has a high capacity for Se(VI), 100 mg/g.[25]

IV. Objectives:

The main goal of this work was to develop models for the packed bed and batch adsorption of oxyanions of selenium onto activated Al_2O_3 and La_2O_3, which may be used for design purposes. Consequently, the model equations should account for the effects of pH; pH_{zpc}; diffusion coefficient; ionic charge and size; specific surface area; Reynolds number; etc. Another important aim of this study is to begin development of a continuous, cyclic process for selenium removal, incorporating the optimum combination of activated Al_2O_3 and La_2O_3. Thus, tests were conducted to determine the best

adsorbents for selenium removal. Process optimization and development is also concerned with determining the concentrations and flowrates which will yield the best results. A data acquisition and control system was designed and implemented during the completion of this project to make future efforts more accurate and easier to scale-up to an industrial situation.

First, the experimental methods, design, and results are given for electrokinetic measurements, and batch and packed bed tests. Next, a great deal of theory was uncovered for use in the batch and packed bed models. A preliminary cost estimate was also made for a continuous mining wastewater treatment process.

V. Experimental Materials. Methods. and Design:

i. Materials:

The physical properties and chemical characteristics of La_2O_3, activated γ-Al_2O_3, and activated α-Al_2O_3 in aqueous solutions effect the adsorption rate; mechanism; and ultimate capacity for different ions. La_2O_3 used in this study was 99.9% pure; had a surface area of 11.84 m^2/g, by BET analysis; and was obtained from ProChem.[26] Particle sizes ranged between 5→20 um. The pH_{zpc} of La_2O_3 was found to be 10.2.[12] Recent studies of the surface structure of La_2O_3 suggest that the majority of active sites consist of peroxide groups, which helps to explain why La_2O_3 has a high pH_{zpc} and a low surface area.[27]

Activated γ-Al_2O_3 used in this study consisted of 1/8 inch porous beads; was 93% Al_2O_3; had a surface area of 350 m^2/g; and was obtained from ADCOA. The pH_{zpc} was

found to be 9.2.[12] Activated α-Al_2O_3 (commercially named DD-6) used in this study consisted of 8x14 mesh porous flakes; was 93% Al_2O_3; had a surface area of 362 m^2/g; and was obtained from Discovery Chemical. The pH_{zpc} is about 9.0. The morphology of activated γ-Al_2O_3 and DD-6 used in this study were observed with a SEM and are shown in Figure 4. The major impurities in activated γ-Al_2O_3 and α-Al_2O_3 are water hydrations and sodium oxide. The active sites on γ-Al_2O_3 and α-Al_2O_3 consist of various surface oxide groups.[15,28,29,30,31]

Figure 4: Morphology of activated γ-Al_2O_3 and DD-6.

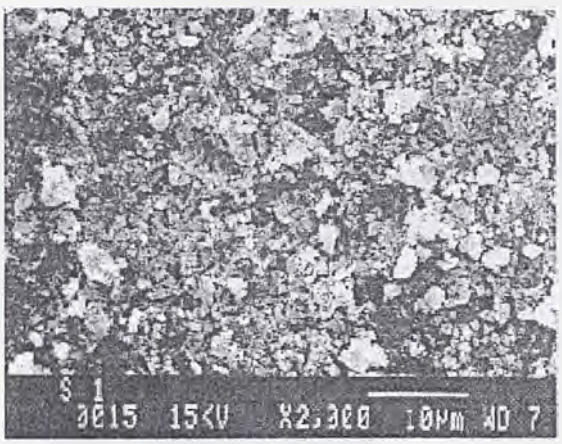

Activated gamma Al_2O_3

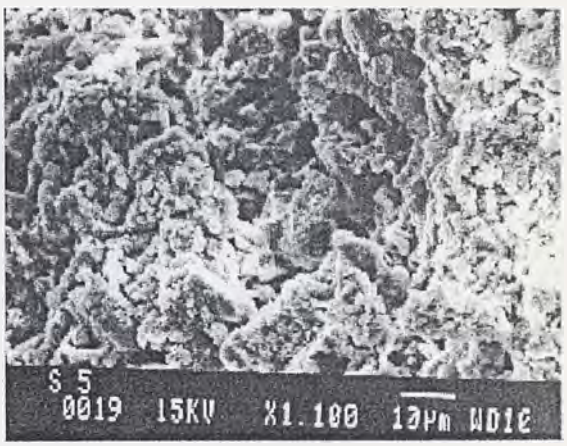

DD-6

ii. Electrokinetic Measurements:

1. Isoelectric Point of Activated γ-Al_2O_3 and La_2O_3:

The isoelectric point (IEP) of metal oxides is often identical with the pH_{zpc}, and is found by simpler methods. The goal of these experiments was to determine the IEP of activated γ-Al_2O_3 and La_2O_3 in the presence of a mixed electrolyte with sulfate ions. The purpose of finding the IEP in the presence of sulfate ions was to observe an increase in

IEP that was reported in the literature to occur for other metal oxides in the presence of sulfate.[32,33]

The method used was to prepare 200 ml of distilled water and add 2 gr of the respective oxide. The mixture was allowed to sit for 30 minutes, then the amount of electrolyte shown in Table IV was added. After the electrolyte addition, the pH was measured as a function of time until steady state was reached. A Corning Model 320 pH/Eh/Temperature meter with an Ag/AgCl electrode was used to measure the pH, Eh, and temperature as a function of time.

Table IV: Electrolyte concentration.

Oxide	Activated γ-Al_2O_3	La_2O_3
Electrolyte Compound	**Electrolyte Molarity**	**Electrolyte Molarity**
Na_2SO_4	0.02	0.02
$CaCl_2$	0.002	0.002
K_2CO_3	0.002	0.002
$NaNO_3$	0.001	0.001

2. Zeta Potential of La_2O_3:

The zeta potential (ζ) of La_2O_3 was measured as a function of pH with a Pen Kem model 501 Lazer Zee Meter, as shown in Figure 5.

Figure 5: Lazer Zee Meter.

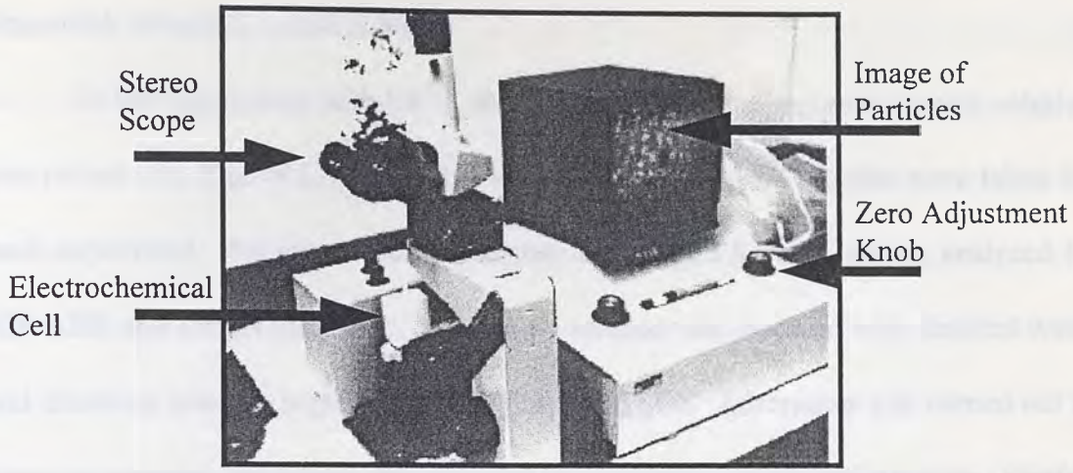

Colloidal solutions were prepared by mixing 25 to 50 mg of La_2O_3 with 50 ml of 10^{-3} M $NaNO_3$ and adjusting the pH with 10^{-3} M HNO_3 and 10^{-2} M NaOH. These solutions were allowed to settle and equilibrate overnight. Then, 25 ml samples were shaken and injected into the electrochemical cell for zeta potential measurement within 1.5 minutes. The zeta potential was found by adjusting the zero knob until the particles appeared stationary without hysteresis. Duplicate measurements were made for each pH and particle concentration, and the average was taken. Particle concentrations were between 500 and 1000 ppm.

iii. Batch Tests:

In the experiments where La_2O_3, activated γ-Al_2O_3, or activated α-Al_2O_3 were used individually, 250 ml of a synthetic selenium solution was mixed with 2 gr of the respective oxide in an Erlenmeyer flask. Ten 10 ml samples were taken for each oxide over a 2 hour period. Samples were immediately filtered and analyzed by ICP-AES.

Adsorption was carried out in a constant temperature shaker bath at 100 rpm (New Brunswick Scientific, model G-86).

In the experiments with $LA^{(T)}$, 200 ml of a synthetic selenium or arsenic solution was mixed with 2 gr of $LA^{(T)}$ in a 250 ml beaker. Four 20 ml samples were taken for each experiment. Samples were immediately centrifuged for one minute, analyzed by ICP-AES, and the pH measured. The arsenic solution was prepared with distilled water and disodium arsenate heptahydrate ($Na_2HAsO_4 \bullet 7H_2O$). Adsorption was carried out at room temperature, and mixing was provided by a magnetic stir bar and stir plate. Stirring speed was adjusted to the onset of a vortex.

All the chemicals used were ACS grade, except for the solid selenium used in the experiments with $LA^{(T)}$. Selenium solution was prepared by dissolving selenium metal in 70% nitric acid; and sodium hydroxide was added to adjust the pH. The reaction of selenium with nitric acid produces selenious acid and a combination of nitrogen monoxide and nitrogen dioxide.[12] The percent relative standard deviation for ICP-AES was 2%.

iv. Packed Bed Tests:

1. Column Design:

Two clear acrylic columns were designed and constructed for the packed bed experiments (Figure 6). The inside diameters are 2.5 inches and the lengths for packing adsorbent are 2 ft. An outer jacket surrounds each column for controlling temperature by water circulation. A top and bottom distributor is connected to each column for inserting

filtering media such as glass wool and membrane filters for fine La_2O_3 particles. Rubber gaskets, threaded rods, hex nuts, and washers flange the distributors to the packed bed section of the columns. One of the columns has sampling ports located 6, 12, and 18 inches from the top of the column, which extend horizontally to the mid-section of the column. Liquid effluent/influent was transported to and from the columns with Masterflex pumps (model # 7521-40, 6-600 rpm; model #7523-30, 1-100 rpm; and two model # 7520-25, 6-600 rpm) using Tygon R-2603 tubing (1/2 inch OD, 5/16 inch ID). Five gallon buckets used for holding liquid were made from HDPE or PVC. A 6 ft. by 5 ft. acrylic containment vessel surrounds the entire experiment.

Figure 6: Packed column design.

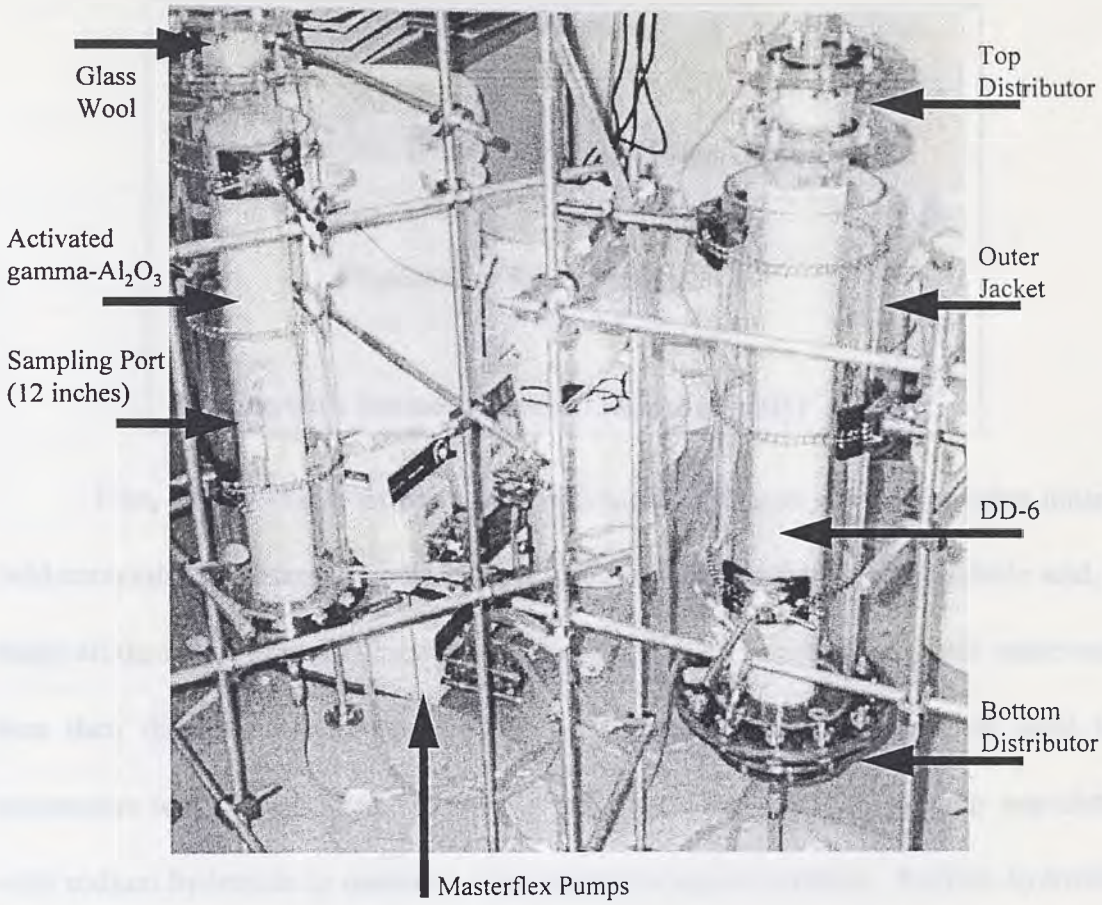

2. Operating Methods and Variables:

The method of each packed bed test varied significantly due to considerations given for the differences in adsorbents or because of improvements which were made. Although the method of conducting each test varied, the operational cycle of events was constant (refer to Figure 7).[8]

Figure 7: Wastewater treatment cycle.

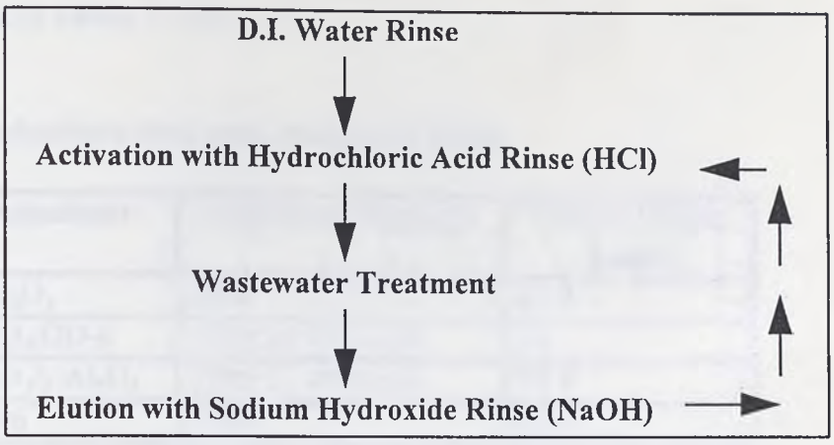

First, the dry adsorbent was rinsed with water to remove any dust or other loosely held contaminants. Next, the column was acidified (activated) with hydrochloric acid, to make all the active sites electropositive. The synthetic or industrial selenium wastewater was then directed through the column until saturation was reached, or until the wastewater was all consumed. Following wastewater treatment, the column was eluted with sodium hydroxide to recover a concentrated selenium solution. Sodium hydroxide was chosen as the regeneration reagent because it has the greatest affinity for the metal oxide surface, when compared to other ions, such as oxyanions of selenium. The hydroxide ions will readily undergo a simple ion exchange mechanism with adsorbed oxyanions of selenium.

The above cycle (excluding the water rinse) was repeated for tests 1 through 4. All the chemicals used were ACS grade, except for the industrial wastewater obtained from ENCYCLE/Texas, which was used in tests 1 through 4. Synthetic selenium stock solutions were prepared by dissolving selenium metal in 70% nitric acid and adding

sodium hydroxide to adjust the pH. The major operating details for each test are summarized in Tables V-VIII:

Table V: Adsorbents used, mass, and packed height.

Test	Adsorbent	Adsorbent Mass (gr)	Packed Height (inches)
1	γ-Al_2O_3	1507	23.9
2	La_2O_3/DD-6	1038, 11.4% La_2O_3	24
3	La_2O_3/γ-Al_2O_3	1535, 11.4% La_2O_3	23.9
4	DD-6	1109	22.9
5	γ-Al_2O_3	1389	22
6	DD-6	1027	21.9

Table VI: pH and temperature characteristics.

Test	pH Wastewater	pH HCl	pH NaOH	Temperature (°C)
1	5.96 ± .02	2.30 ± .02	11.82 ± .02	23 ± 1
2	5.94 ± .02	2.17 ± .02	11.82 ± .02	23 ± 1
3	5.95 ± .02	1.08 ± .02	13.68 ± .02	23 ± 1
4	12.16 ± .16	1.10 ± .03	13.27 ± .03	23 ± 1
5 and 6	3.69 ± .14	0.91 ± .03	13.53 ± .05	23 ± 1

Table VII: Wastewater characteristics.

Test	Inlet Selenium Concentration (ppm)	Other Characteristics
1	0.594 ± .012	As,Cd,Cr,Cu,Ni,Pb,Zn,High Sodium and Heavy Metals
2	0.594 ± .012	As,Cd,Cr,Cu,Ni,Pb,Zn,High Sodium and Heavy Metals
3	0.594 ± .012	As,Cd,Cr,Cu,Ni,Pb,Zn,High Sodium and Heavy Metals
4	0.1082 ± .0022	As,Cd,Cr,Cu,Ni,Pb,Zn,High Sodium, Low Heavy Metals
5 and 6	86.9 ± 7.1	Tap Water

Table VIII: Mode of flow for each step in the operating cycle.

Test	Water Rinse	HCl Rinse	Wastewater Rinse	NaOH Rinse
1	Downflow	Downflow	Downflow	Downflow
2	Downflow	Downflow	Downflow	Downflow
3	Upflow	Upflow	Downflow	Upflow
4	Downflow	Downflow	Downflow	Downflow
5	Downflow	Downflow	Downflow	Downflow
6	Downflow	Downflow	Downflow	Downflow

In tests 1 through 3, downflow mode was conducted in such a manner that the wastewater percolated through the column, which led to channeling. A major consequence of channeling was that the adsorbent surface area was not fully utilized, meaning that these tests cannot provide quantitative information about adsorbent performance. In tests 4 through 6, downflow was run in plug flow mode by maintaining a head of liquid at the top of the column and manually adjusting the inlet pump speed to equal the outlet pump speed. Plug flow insured that all of the adsorbent surface area was wetted and thus available for adsorbing selenium ions from the wastewater. However, maintaining plug flow manually is difficult to control because of drift in the inlet and outlet pump speeds, which often caused the liquid level to fluctuate below and above the adsorbent height.

The first test used γ-Al_2O_3 with a trace amount of La_2O_3. The La_2O_3 was present in trace amounts ($\approx$ 2 grams) because the filter did not retain the La_2O_3 particles, causing them to be washed out with water before the experiment actually began. The remaining La_2O_3 particles were either trapped in the pores of the γ-Al_2O_3 or lodged against the sides/bottom area of the column.

Besides the difficulties in retaining the La_2O_3 in the packed bed, the small particle size also increases the pressure drop by three orders of magnitude (calculated by using the Ergun equation for packed beds). Therefore, in a bed packed with La_2O_3, the tendency is for the liquid to form channels to reduce the resistance to flow (Darcy's Law states that flow in porous media will be in the direction of minimum pressure drop). Thus, poor solid/liquid contact made the packed bed experiments with a mixture of activated Al_2O_3 and La_2O_3 difficult to operate.

In the second cycle of test 3, the temperature of the column was increased to about 50 °C during elution with NaOH by passing hot water through the outer jacket. This procedure was used to determine whether high temperature would improve the rate and efficiency of eluting the adsorbed selenium ions from the surface.

3. Data Acquisition and Control for Packed Beds:

Due to difficulties in controlling and measuring the liquid level, flowrate, temperature, and pH for the packed bed system shown in Figure 6, a data acquisition and control system was developed and constructed for future experiments. This setup will also make operating two experiments at a time more feasible, accurate, and expedient. The major hardware and software that was purchased are listed with their major functions and specifications in Table IX.

Table IX: Hardware and software purchased for data acquisition and control.

Data Shuttle for A/D or D/A Transfer	**Description**
General Description	Accommodates 8 analog inputs, 2 analog outputs (4-20 mA or different voltage ranges); and 8 digital I/O lines.
Resolution Analog in	12-bit.
Sensor Types	Thermocouple, mV, V.
WorkBench for Windows Software	**Description**
General Description	Measuring, process control, and analyzing software for Windows.
Functions	x-y graphing; y-t graphing; PID control; RS-232 serial interface; etc.
Data Collection	Uninterrupted while using other programs.
DDE	Dynamic data exchange for real-time export to other applications supporting the DDE protocol; i.e. Excel may be used to start and control WorkBench during an experiment.
Measuring, Control, and Analysis	A/D, D/A converters; Pre/Post and Start/Stop triggers; digital I/O's; mathematics (arithmetic to calculus); etc.
Computer Equipment	**Description**
General Description	Computer, monitor, and Windows software.
Computer	Intel 66 Mhz 80486DX2 microprocessor; 8 MB DRAM expandable to 64 MB; 540 MB Western Digital IDE (13ms); 17 MB DTR; Integrated local-bus accelerated graphics with 1 MB DRAM.
Flowmeters	**Description**
General Description	Flowmeters generate an electrical signal proportional to flowrate. Flowmeters are linear from 13 to 100 ml/min. A 7-um filter is recommended to prevent damage to sensor.
SS Parts Replaced With Kynar	HCl will not corrode Kynar as quickly as SS.
Media Compatibility	Resistant to strong acids and bases (NaOH and HCl), at least pH 1-14.
Output	0-5 VDC for datalogging.
Accuracy	± 3% of full scale.
Linearity	± 3% of full scale.
Operating Temperature	0-50 °C
Maximum Pressure	100 psi at 20 °C

A schematic of the data acquisition and control scheme is shown in Figure 8. Magnetic reed float switches are connected to a relay box which converts an on or off 120 VAC signal powered from the wall socket to a TTL (Transistor to Transistor Logic) input signal to the Data Shuttle (A/D or D/A converter). The Data Shuttle converts the analog input signal to a digital signal, which is used by the software on the computer to record the measured signal and implement a control action. The control action is to either increase or decrease the inlet pump speed, depending on whether the liquid level is too high or too low. In order to change the pump speed, the software on the computer sends a digital signal to the Data Shuttle, which converts it to a 4-20 mA analog signal and sends it to the pump. Turbine wheel flowmeters are positioned to relay the flowrates of the effluent streams of each column to the computer. The effluent pumps are adjusted manually to reach a desired set point flowrate with the aid of an LED bar graph display.

The effluent flowrate data is integrated continuously to obtain the total volume treated, and this data is also used by the control algorithm. PID (Proportional, Integral, Derivative) control requires a measured signal, set point, and three tuning parameters for the controller. Liquid height may be calculated from the input and output flowrates, the effective area, and time as follows:

$$h = h_{ss} + \int_0^t \frac{(q_i - q_o)}{A_e} dt \tag{32}$$

Figure 8: Data acquisition and control system for packed beds.

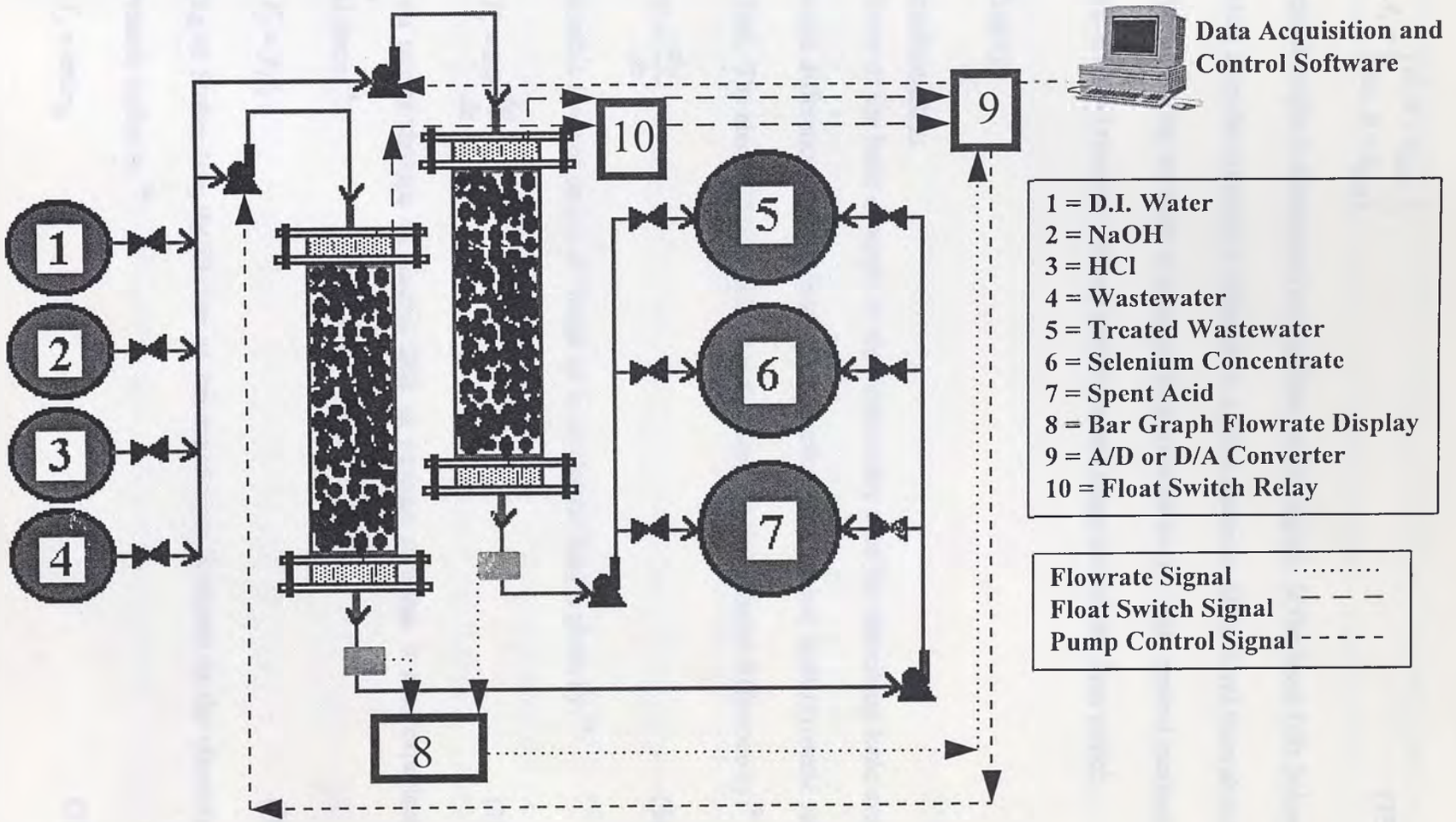

$$A_e = \begin{cases} A, h > h_{solid} \\ A\varepsilon, h < h_{solid} \end{cases} \quad (33)$$

The set point height is determined by the float switch signal. If the level falls below the float switch, then the set point is changed to a point above it. If the level rises above the float switch, then the set point is changed to a point below it. This control method will insure that the level remains within a predetermined range around the float switch.

VI. Theory:

i. Electrochemistry:

Some of the basic concepts in electrochemistry used for describing ionic systems are potential difference; electric field; force; friction; drift speed; hydrodynamic radius; and ion flux. The electric field is related to the electrostatic potential difference by:[34]

$$E = \frac{d\psi}{dx} \quad (34)$$

The coulombic force on an ion of charge $z_j e$ in an electric field is given by:[34]

$$F_j = z_j e \frac{d\psi}{dx} \quad (35)$$

As an ion moves through an electric field in aqueous solution, it also experiences a frictional force:[34]

$$F_j' = f_j s_j' \quad (36)$$

According to Stokes law, the friction an ion experiences is related to the viscosity and hydrodynamic radius by:[34]

$$f_j = 6\pi u r_{Hj} \quad (37)$$

The hydrodynamic radius is the effective radius of an ion in solution, taking into account all of the water molecules it carries in its hydration sphere. Small ions give rise to stronger electric fields than larger ones because the electric field at the surface of a sphere of radius r is proportional to $z_j e/r_j^2$: thus, the smaller the radius, the stronger the electric field. Therefore, small ions, which are more solvated than big ones, have a larger hydrodynamic radius. The drift speed of an ion is found by setting the frictional force equal to the force from an electric field as below:[34]

$$s_j = \frac{z_j eE}{f_j} \tag{38}$$

The ion flux is a function of the drift speed and concentration of ions per unit area.[34]

ii. Electrokinetics:

Electrokinetic theory is used in ionic systems where mass transfer is taking place due to the force exerted on an ion diffusing to the active sites on the charged surface of the adsorbent. The forced diffusion term is very important in ionic systems, where a major external force on an ion is equal to the product of the ionic charge and the local electric field strength. Each ionic species may thus be under the influence of a different force.[35]

The most useful relationships in electrokinetic theory are derived from the concept of the electric double layer. The electric double layer refers to two separate layers of charge that exist on the oxide surface and in the diffuse region extending into the solution. Thus, the electric double layer is just the arrangement of positive and

negative charges on the surface and the charges in the liquid phase at the interface between the solid and liquid phases.[15,36]

The Stern treatment of the electric double layer was invented to avoid the assumption of point charges and consequent neglect of the ionic radius. Stern guessed that the surface would consist of two parts:[15]

1. A layer of ions adsorbed at the surface and forming an inner compact double layer.
2. A diffuse layer.

The overall picture presented by Stern is a compact layer of thickness δ in which $d\psi/dx$ is approximated by $(\psi_0-\zeta)/\delta$. For the conditions encountered in wastewater treatment, the ionic strength is sufficiently high to make ζ approximately equal to zero.[15]

Charges in the region bounded by δ respond to four forces:

1. Electric potential.
2. Diffusion force, tending to smooth out concentration variations.
3. Desolvation.
4. The bulk movement of charge carried along by the flow of the liquid.

The electric potential is created by layers of charge between the surface of the solid adsorbent and the solution. The diffusion force is due to a concentration gradient. The bulk movement of the liquid is governed by shear and pressure forces. The surface of shear is an imaginary surface which is considered to lie close to the solid surface and within which the fluid is stationary. The average potential in the surface of shear is the zeta potential, or electrokinetic potential. The shear plane is located at the outer edge of the inner part of the double layer. This concept is limited when dealing with rough

surfaces, where a simple geometric configuration and Newtonian flow are usually assumed. The desolvation force is due to the loss of water molecules from an ion's hydration sphere as it moves toward a highly charged oxide surface, such as activated Al_2O_3 or La_2O_3.[15]

Furthermore, there are four general mechanisms of charge development at the solid/liquid interface:[15]

1. Differences in the affinity of the two phases for ions of one charge or the other. This includes adsorption of ions onto the solid from solution.
2. Ionization of surface groups.
3. Differences in the affinity of the two phases for electrons.
4. Physical entrapment of non-mobile charge in one phase.

Parts 1 and 2 of the above list are mainly responsible for charge development on activated Al_2O_3 and La_2O_3. From part 1 of the above list, there are three classes of ions that interact with the surface:[15]

i. Potential determining ions, mainly H^+ and OH^- for activated Al_2O_3 and La_2O_3.
ii. Indifferent ions, such as K^+ and NO_3^-. These are called indifferent because they will not react with the surface, but are held near it by coulombic attraction.
iii. Specifically adsorbed ions.

Adsorption of an ion by forces other than coulombic attraction or repulsion is specific adsorption. The forces could be chemical or physical. If chemical forces are involved, adsorption must occur into the inner or compact part of the double layer. Specifically adsorbed ions can reverse the sign of the zeta potential, ζ, whereas indifferent ions can only reduce ζ asymptotically to zero. A physically adsorbed ion does

not affect the pH_{zpc}, but can reverse the sign of ζ. A chemisorbed ion shifts the pH_{zpc} or IEP and can remain adsorbed even when the underlying surface has the same sign itself. Thus, one part of solving a problem that involves electrokinetic phenomena is to classify all ionic species as potential determining, indifferent, or ones that enter the inner part of the double layer and undergo a specific interaction with the surface.[15]

iii. Thermodynamics of Adsorption:

The free energy of adsorption for charged ions onto highly charged metal oxides is due to three main contributions: a specific chemical interaction; coulombic attraction or repulsion; and desolvation of the ion.[20,28]

$$\Delta G_{ads,j} = \Delta G_{chem,j} + \Delta G_{coul,j} + \Delta G_{ds,j} \tag{39}$$

By including all three free energy terms, it is possible to explain how some ions adsorb better than others onto metal oxides. The main contribution to the specific chemical interaction is between the adsorbing ion and the amphoteric surface hydroxyl groups. The chemical free energy is a function of the bulk concentration; number and nature of surface vacant sites; pH of the solution; temperature; etc.

The surface charge of the oxides can be predicted using the conventional zero point of charge concept in conjunction with the solution pH and Nernst equation:[28]

$$\psi_0 = \frac{2.3RT}{F}\left(pH_{zpc} - pH\right) \tag{40}$$

Equation (40) shows that the surface charge is higher for oxides with high pH_{zpc} values at a given pH, and that the surface makes a transition from positive to negative charge above the pH_{zpc}. The coulombic free energy contribution is dependent upon the surface charge and charge of the ion, as shown below:

$$\Delta G_{coul,j} = 2.3 z_j RT\left(pH_{zpc} - pH\right) \tag{41}$$

The desolvation energy is due to ions losing part of their hydration sheaths as they approach and attach to the highly charged metal oxide surface. The desolvation energy is a function of ionic charge; ionic radius; and the dielectric constant of the interface. This energy is nearly the same in magnitude as the coulombic free energy, but is always positive and deleterious to adsorption for positive or negative ions. Max Born developed the fundamental differential equation governing the energy of desolvation below:[20]

$$dG_{ds,j} = -\frac{1}{2}\bar{x} \bullet \bar{D}\, dV \tag{42}$$

$$\bar{D} = \frac{z_j e}{4\pi r_j^2} \tag{43}$$

$$\bar{x} = \frac{z_j e}{4\pi \varepsilon_o \varepsilon_r r_j^2} \tag{44}$$

Assuming that ions maintain a spherical structure during the adsorption process, the differential equation for the free energy of desolvation is as follows:

$$dG_{ds,j} = \frac{-\left(z_j e\right)^2 N_A\, dr_j}{8\pi \varepsilon_o \varepsilon_r r_j^2} \tag{45}$$

iv. Mass Transport Mechanism:

The advantage of using a transport mechanism to describe the uptake of ions as a function of time is that it is primarily phenomenological in nature and the exact interfacial reaction at the surface is not required. This point is essential when modeling the adsorption of a large matrix of ions because the type of reaction may vary for each ion. Figure 9 illustrates the physical and chemical phenomena taking place during adsorption onto the metal oxides. In line with the thermodynamics, there is a concentration, potential, and ionic radii gradient. The ionic flux due to the concentration and potential gradients are described by the Nernst-Planck flux equations.[37] The ionic flux due to the radii gradient is found by combining equation (45) with rules from electrochemistry.

Figure 9: Transport of oxyanions of Se (IV) to the oxide-water interface.

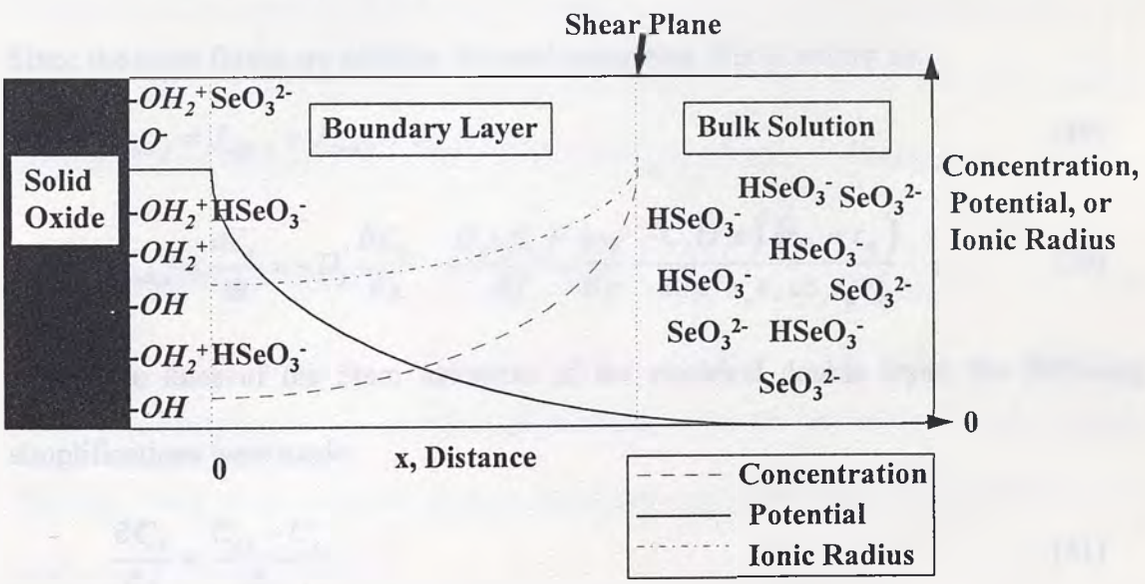

First, the molar force due to desolvation is given as follows:[34]

$$F_{ds,j} = \frac{dG_{ds,j}}{dx} = \frac{-(z_j e)^2 N_A \, dr_j}{8\pi\varepsilon_o\varepsilon_r r_j^2 \, dx} \approx \frac{(z_j e)^2 N_A (r_{Hj} - r_{ej})}{8\pi\varepsilon_o\varepsilon_r \delta_j r_{ej} r_{Hj}} \tag{46}$$

Essentially, the right side of equation (46) suggests that the ionic radius gradient can be approximated by a straight line with a boundary layer thickness particular to each ion. Where the radius of an ion in the bulk solution is its hydrated radius and the radius of the adsorbed ion is nearly its crystallographic radius. From electrochemistry, the following relationships are found between molar force; speed; friction; concentration; and flux.[34]

$$N_A f_j s_j' = F_{ds,j} = \frac{-N_A f_j J_{ds,j}}{C_j} \tag{47}$$

Furthermore, since friction is a function of the decreasing ionic radii; Stokes law may be combined with equations (46) and (47) to obtain the desolvation flux as follows:

$$J_{ds,j} = \frac{-C_j (z_j e)^2 (r_{Hj} - r_{ej})}{48\pi^2\varepsilon_o\varepsilon_r u \delta_j r_{ej} r_{Hj}^2} \tag{48}$$

Since the ionic fluxes are additive, the total adsorption flux is written as:

$$J_{ads,j} = J_{diff,j} + J_{coul,j} + J_{ds,j} \tag{49}$$

$$J_{ads,j} = \frac{d\Gamma_j}{dt} = -D_j \frac{\partial C_j}{\partial x} - \frac{D_j z_j C_j F}{RT} \frac{\partial \psi}{\partial x} - \frac{C_j (z_j e)^2 (r_{Hj} - r_{ej})}{48\pi^2\varepsilon_o\varepsilon_r u \delta_j r_{ej} r_{Hj}^2} \tag{50}$$

Along the lines of the Stern treatment of the electrical double layer, the following simplifications were made:

$$\frac{\partial C_j}{\partial x} \approx \frac{C_{s,j} - C_j}{\delta_j} \tag{51}$$

$$\frac{\partial \psi}{\partial x} \approx \frac{\psi_o}{\delta_j} \tag{52}$$

Also, three constants are defined to obtain the loading rate expression given by equation (56):

$$a_j = \frac{(z_j e)^2 (r_{Hj} - r_{ej})}{48\pi^2 \varepsilon_o \varepsilon_r u r_{ej} r_{Hj}^2} \tag{53}$$

$$k_j = \frac{D_j}{\delta_j} \tag{54}$$

$$k_{aj} = \frac{a_j}{\delta_j} \tag{55}$$

$$\frac{dC_{s,j}}{dt} = -A_{sp} C_s \left[k_j (C_{s,j} - C_j) + \frac{k_j z_j C_j F \psi_0}{RT} + C_j k_{aj} \right] \tag{56}$$

Where, k_j is a diffusion-based mass transfer coefficient due to a concentration and potential gradient and k_{aj} is a mass transfer coefficient due to an ionic size gradient between the bulk ionic radii (hydrated radius) and the surface-attached size.

v. Mathematical Modeling:

1. Batch Adsorption:

The batch model is simpler mathematically than the packed bed model because the total mass at any time is equal to the initial mass and is distributed between the surface and the bulk solution.

$$C_{s,j} = C_{o,j} - C_j \tag{57}$$

$$J_{ads,j} = \frac{d\Gamma_j}{dt} = \frac{-1}{A_{sp}C_s}\frac{dC_j}{dt} = \frac{1}{A_{sp}C_s}\frac{dC_{s,j}}{dt} \tag{58}$$

$$\alpha_j = \frac{C_j}{C_{o,j}} \tag{59}$$

$$\frac{d\alpha_j}{dt} = A_{sp}C_s\left[k_j\left(1-2\alpha_j\right)+\frac{k_j z_j F\alpha_j\psi_o}{RT}+k_{aj}\alpha_j\right] \tag{60}$$

Equation (60) is nonlinear, due to the second term in brackets. To obtain an analytical solution, equations (40) and (60) combined were linearized with a first order Taylor expansion and substitutions made as follows:

$$\alpha_i\psi_o \approx \psi_{o,ss} + \psi_{o,ss}\left(\alpha_i - 1\right)+\left(\psi_o - \psi_{o,ss}\right) \tag{61}$$

$$\psi_o \approx \frac{RT}{F}\left(\alpha_{H^+} - 1\right)+\psi_{o,ss} \tag{62}$$

$$w_j = k_j\left(1 - z_j\right) \tag{63}$$

$$v_j = k_{aj} + \frac{k_j z_j F\psi_{o,ss}}{RT} - 2k_j \tag{64}$$

$$\frac{d\alpha_j}{dt} = A_{sp}C_s\left(w_j + \alpha_j v_j + k_j z_j \alpha_{H^+}\right) \tag{65}$$

The fraction remaining of each species is tied together by a dependence on the fraction remaining of the hydrogen ion in equation (65). The solution to equation (65) takes on the same form for all species except hydrogen, and was found by using Laplace transforms. The final equations are as follows:

$$\alpha_{H^+} = \kappa\, exp\left(\frac{-t}{\tau_{H^+}}\right) + \alpha_{H^+,ss} \tag{66}$$

$$\tau_{H^+} = \frac{-1}{A_{sp} C_s \left(v_{H^+} + k_{H^+} z_{H^+} \right)} \tag{67}$$

$$\kappa = \frac{w_{H^+} + v_{H^+} + k_{H^+} z_{H^+}}{v_{H^+} + k_{H^+} z_{H^+}} \tag{68}$$

$$\alpha_{H^+,ss} = \frac{-w_{H^+}}{v_{H^+} + k_{H^+} z_{H^+}} \tag{69}$$

$$\alpha_j = \frac{\left(\alpha_{j,ss} - 1 \right)}{\left(\tau_{H^+} - \tau_j \right)} \left[\tau_j \, exp\left(\frac{-t}{\tau_j} \right) - \tau_{H^+} \, exp\left(\frac{-t}{\tau_{H^+}} \right) \right] + \alpha_{j,ss} \tag{70}$$

$$\tau_j = \frac{-1}{A_{sp} C_s v_j} \tag{71}$$

$$\alpha_{j,ss} = \frac{\kappa k_j z_j}{v_j} + 1 \tag{72}$$

Since the charge of the hydrogen ion is one, the theoretical values for κ and $\alpha_{H+,ss}$ are one and zero in equations (68) and (69), respectively.

2. Packed Bed Adsorption:

The concentration in the column and, hence, the degree of saturation of the adsorbent, is a function of volume treated and bed length. With the above, and assuring that axial diffusion is negligible, the following partial differential equation has been essentially arrived at previously by various workers to describe concentration in a packed bed as a function of volume treated and bed length:[38]

$$\varepsilon \frac{\partial C_j}{\partial V} + \frac{\rho_B}{C_s} \frac{\partial C_{s.j}}{\partial V} + \frac{1}{A} \frac{\partial C_j}{\partial L} = 0 \tag{73}$$

The loading rate expression required to solve equation (73) is given by equation (56), with time replaced by volume and flowrate.

$$\frac{dC_{s.j}}{dV} = \frac{-A_{sp} C_s}{q_o} \left[k_j \left(C_{s.j} - C_j \right) + \frac{k_j z_j C_j F \psi_0}{RT} + C_j k_{aj} \right] \tag{74}$$

An approximate analytical solution was found by linearizing the second term in brackets in equation (74), taking the Laplace transforms of equations (73) and (74) to solve for bulk concentration, and inverting back to the time domain with a sixth order approximation.

The linearization of the second term in brackets in equation (74) is given by a first order Taylor expansion as follows:

$$C_j \psi_0 \approx \left(C_j \psi_0 \right)_{ss} + C_{j,ss} \left(\psi_0 - \psi_{0,ss} \right) + \psi_{0,ss} \left(C_j - C_{j,ss} \right) \tag{75}$$

$$\psi_0 \approx \psi_{0,ss} + \frac{RT \left(C_{H^+} - C_{H^+,ss} \right)}{F C_{H^+,ss}} \tag{76}$$

The Laplace domain solution to equations (73) and (74) for all ionic species except hydrogen is given by:

$$\tilde{C}_j = \frac{C_{0,j}}{s}\exp\left(\frac{\gamma_j sL}{s+\lambda_j}\right)\exp(-A\varepsilon sL) \tag{77}$$

$$\lambda_j = \frac{k_j A_{sp} C_s}{q_o} \tag{78}$$

$$\lambda_{aj} = \frac{k_{aj} A_{sp} C_s}{q_o} \tag{79}$$

$$\gamma_j = \frac{A\rho_B}{C_s}\left[\lambda_{aj} - \lambda_j\left(1 - 2.3z_j\left(pH_{zpc} - pH_0\right)\right)\right] \tag{80}$$

If the middle exponential term in equation (77) is approximated by a sixth order Taylor expansion, the following solution is obtained:

$$\frac{C_j}{C_{0,j}} = \left[1 + \left(c_{1j} + c_{2j}V_o + c_{3j}V_o^2 + c_{4j}V_o^3 + c_{5j}V_o^4 + c_{6j}V_o^5\right)\exp\left(-\lambda_j V_o\right)\right] \tag{81}$$

$$V_o = V - \varepsilon AL \tag{82}$$

$$\sigma_j = \gamma_j L \tag{83}$$

$$c_{1j} = \sum_{n=1}^{6}\frac{\sigma_j^n}{n!} \tag{84}$$

$$c_{2j} = -\lambda_j\left[\sum_{n=2}^{6}\frac{\sigma_j^n(n-1)}{n!}\right] \tag{85}$$

$$c_{3j} = \frac{\lambda_j^2}{2}\left[\frac{\sigma_j^3}{6} + \frac{\sigma_j^4}{8} + \frac{\sigma_j^5}{20} + \frac{\sigma_j^6}{72}\right] \tag{86}$$

$$c_{4j} = \frac{-\lambda_j^3}{6}\left[\frac{\sigma_j^4}{24} + \frac{\sigma_j^5}{30} + \frac{\sigma_j^6}{72}\right] \tag{87}$$

$$c_{5j} = \frac{\lambda_j^4}{24}\left[\frac{\sigma_j^5}{120} + \frac{\sigma_j^6}{144}\right] \tag{88}$$

$$C_{6j} = \frac{-\lambda_j^5 \sigma_j^6}{86{,}400} \tag{89}$$

This solution suggests that the modeled bulk concentration of a species can be found as a function of volume treated if the two mass transfer coefficients given by equations (54) and (55) are known.

VII. Results:

i. Electrokinetic Measurements:

The IEP of activated γ-Al_2O_3 in 0.02 M sulfate is 9.8 according to Figure 10. This is about 0.6 pH units higher than the IEP found in the presence of indifferent ions. The IEP of La_2O_3 in 0.02 M sulfate is at least 11.32, according to Figure 10. This is about 1.1 to 1.9 pH units higher than the IEP found in the presence of indifferent ions. Thus, the results of Figure 10 compared with previous workers' findings in the presence of indifferent ions show that sulfate is a chemisorbed ion on activated γ-Al_2O_3 and La_2O_3 because it shifts the IEP.[28]

Zeta potential measurements of La_2O_3 in 10^{-3} M $NaNO_3$ on Figure 11 show that the La_2O_3 particles are electropositive below the pH_{zpc} and electronegative above the pH_{zpc}. The pH_{zpc} of 9.4 shown on Figure 11 is slightly lower than previous workers' findings. However, the pH_{zpc} of La_2O_3 is nevertheless higher than activated Al_2O_3.

Figure 10: IEP of La_2O_3 and activated gamma Al_2O_3 in 0.02 M sulfate.

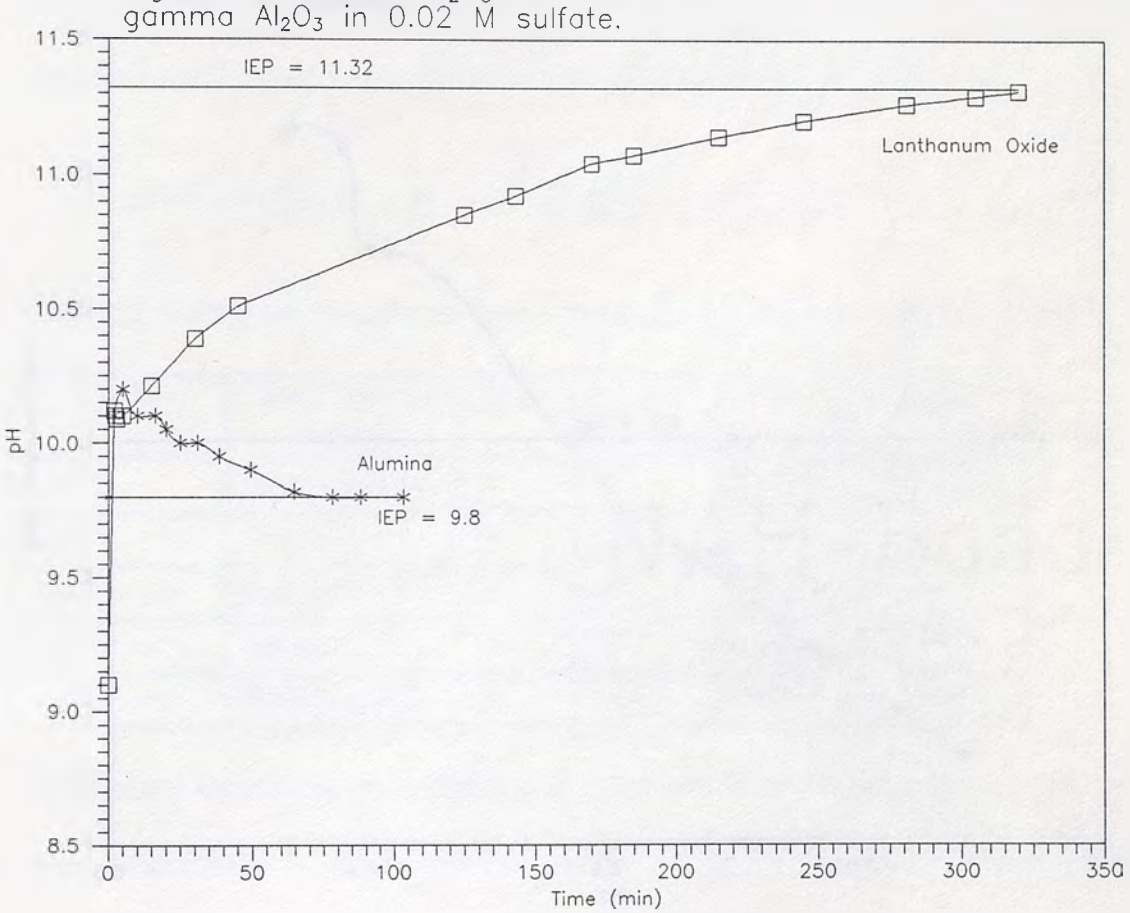

Figure 11: Zeta potential of La_2O_3 as a function of pH.
— 10^{-3} M $NaNO_3$.

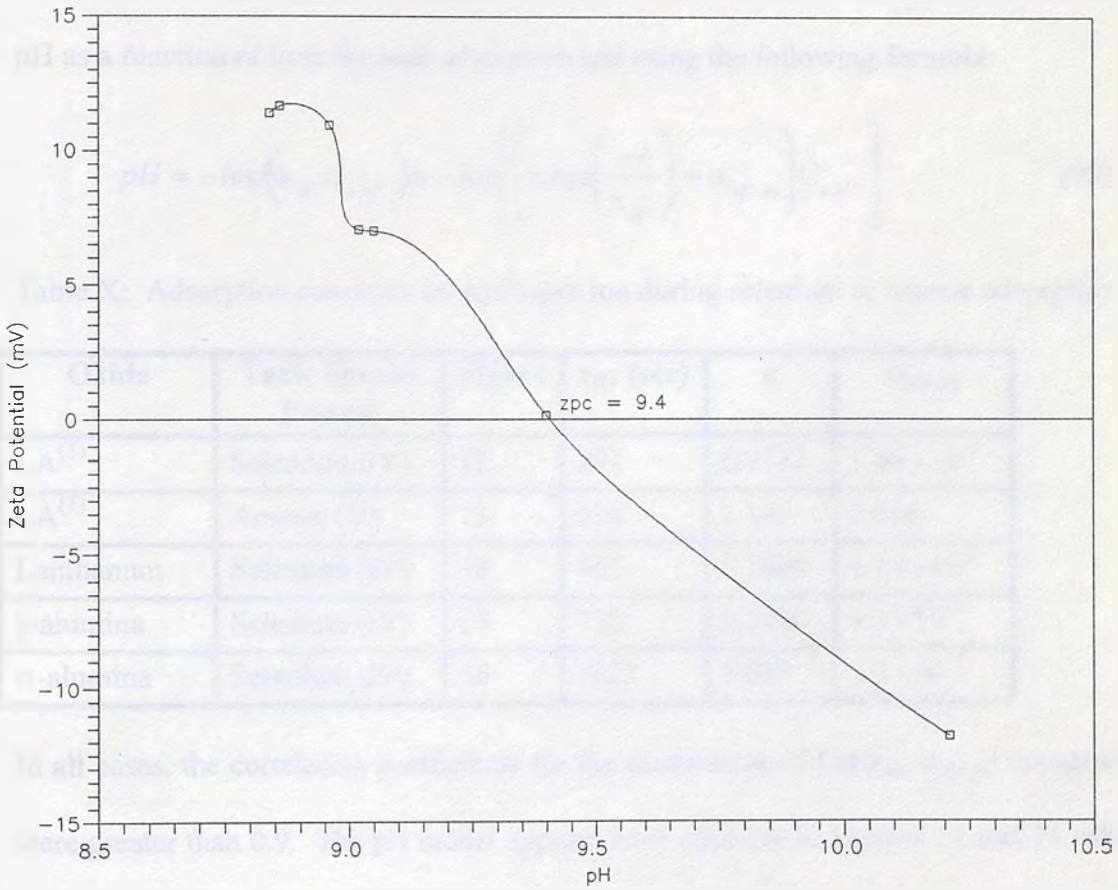

Therefore, La_2O_3 is more electropositive than activated Al_2O_3 and should be a better adsorbent for negative ions such as oxyanions of selenium. The pH measurement errors in these experiments could have been eliminated by using a dedicated reference electrode, and using lower particle concentrations.

ii. Batch Tests:

The constants for hydrogen ion adsorption in Table X below were obtained by linear regression of equation (66), and the modeled pH was plotted versus experimental pH as a function of time for each adsorption test using the following formula:

$$pH = -log\left(\alpha_{H^+} C_{o,H^+}\right) = -log\left[\left(\kappa\, exp\left(\frac{-t}{\tau_{H^+}}\right) + \alpha_{H^+,ss}\right) C_{o,H^+}\right] \qquad (90)$$

Table X: Adsorption constants for hydrogen ion during selenium or arsenic adsorption.

Oxide	Toxic Species Present	Figure	τ_{H+} (sec)	κ	$\alpha_{H+,ss}$
$LA^{(T)}$	Selenium (IV)	12	293	0.1142	1.66×10^{-3}
$LA^{(T)}$	Arsenic (V)	13	516	1.145	0.016
Lanthanum	Selenium (IV)	14	462	0.1605	1.19×10^{-3}
γ-alumina	Selenium (IV)	15	732	0.7406	9.3×10^{-4}
α-alumina	Selenium (IV)	16	1015	1.059	3.0×10^{-4}

In all cases, the correlation coefficients for the linear plots of $Ln(\alpha_{H+}-\alpha_{H+,ss})$ versus time were greater than 0.9. The pH model appears least effective in Figures 12 and 14, which both had correlation coefficients of 0.9 in their linear fraction remaining forms. In Table X, the κ constants for the modeled curves on Figures 13, 15, and 16 approached the

Figure 12: Adsorption of biselenite by $LA^{(T)}$.
– Temperature 27 degrees celsius.
– Initial concentration 14.4 ppm Se.
– Stirring speed adjusted to onset of vortex.

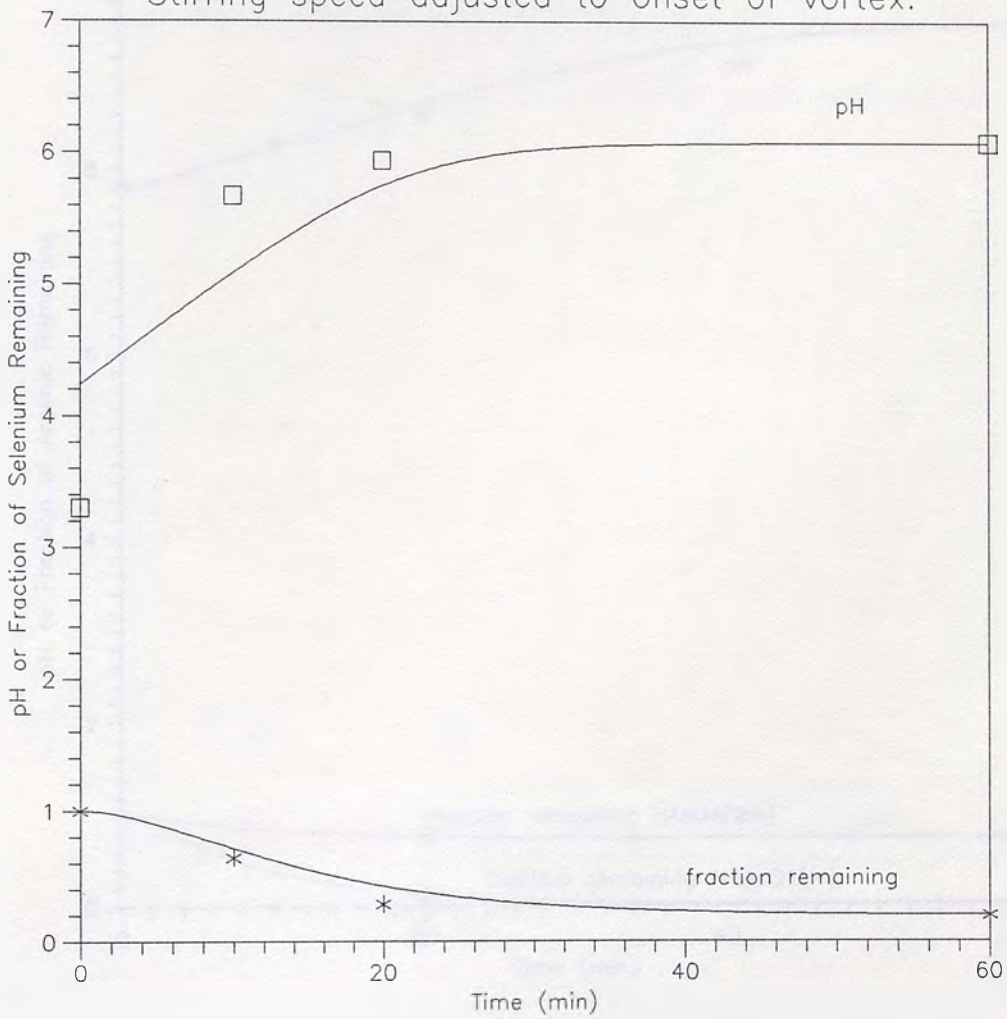

Figure 13: Adsorption of arsenic by $LA^{(T)}$.
- Temperature 26 degrees celsius.
- Initial concentration of As in $HAsO_4^{2-}$ 3.62 ppm.
- Initial concentration of As in $H_2AsO_4^-$ 0.51 ppm.
- Stirring speed adjusted to onset of vortex.

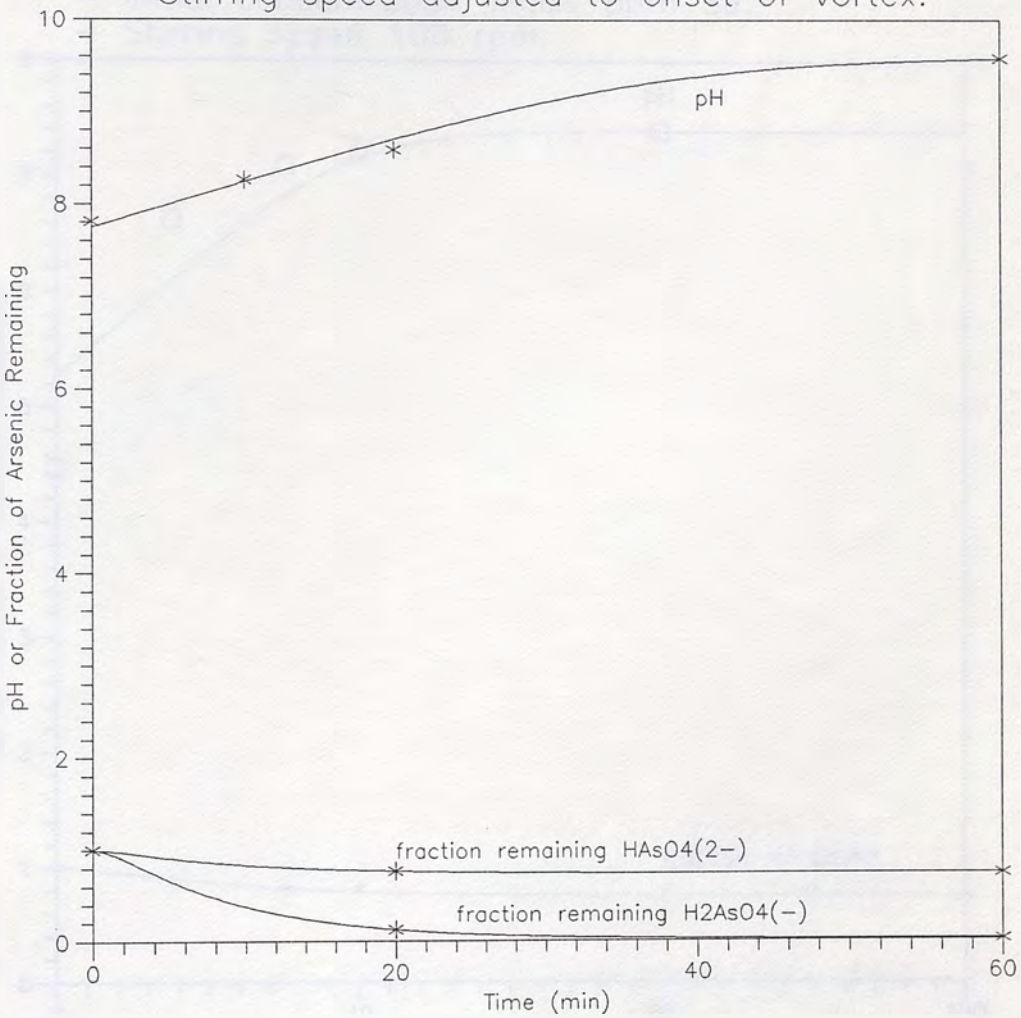

Figure 14: Adsorption of biselenite by La_2O_3.
- Temperature 28 degrees celsius.
- Initial concentration 77.61 ppm Se.
- Stirring speed 100 rpm.

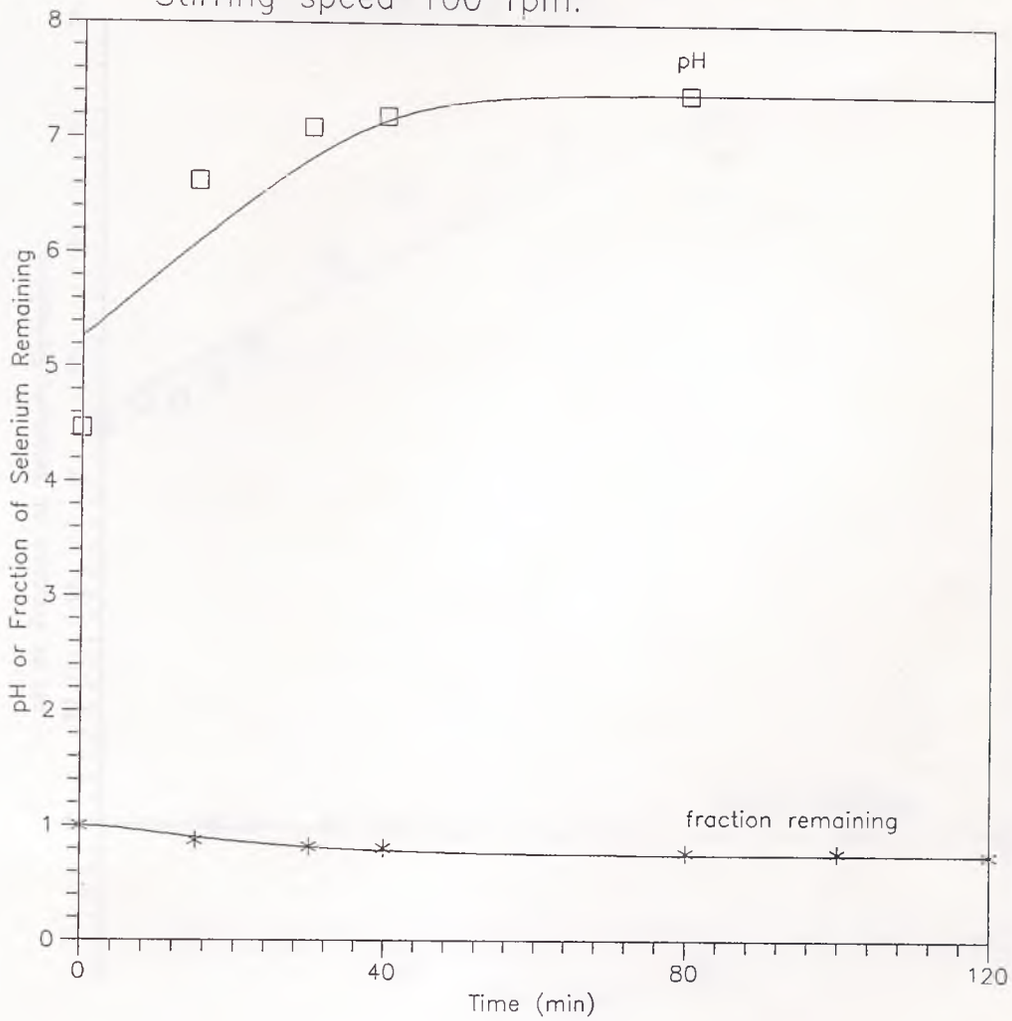

Figure 15: Adsorption of biselenite by gamma–Al_2O_3.
– Temperature 28 degrees celsius.
– Initial concentration 77.61 ppm Se.
– Stirring speed 100 rpm.

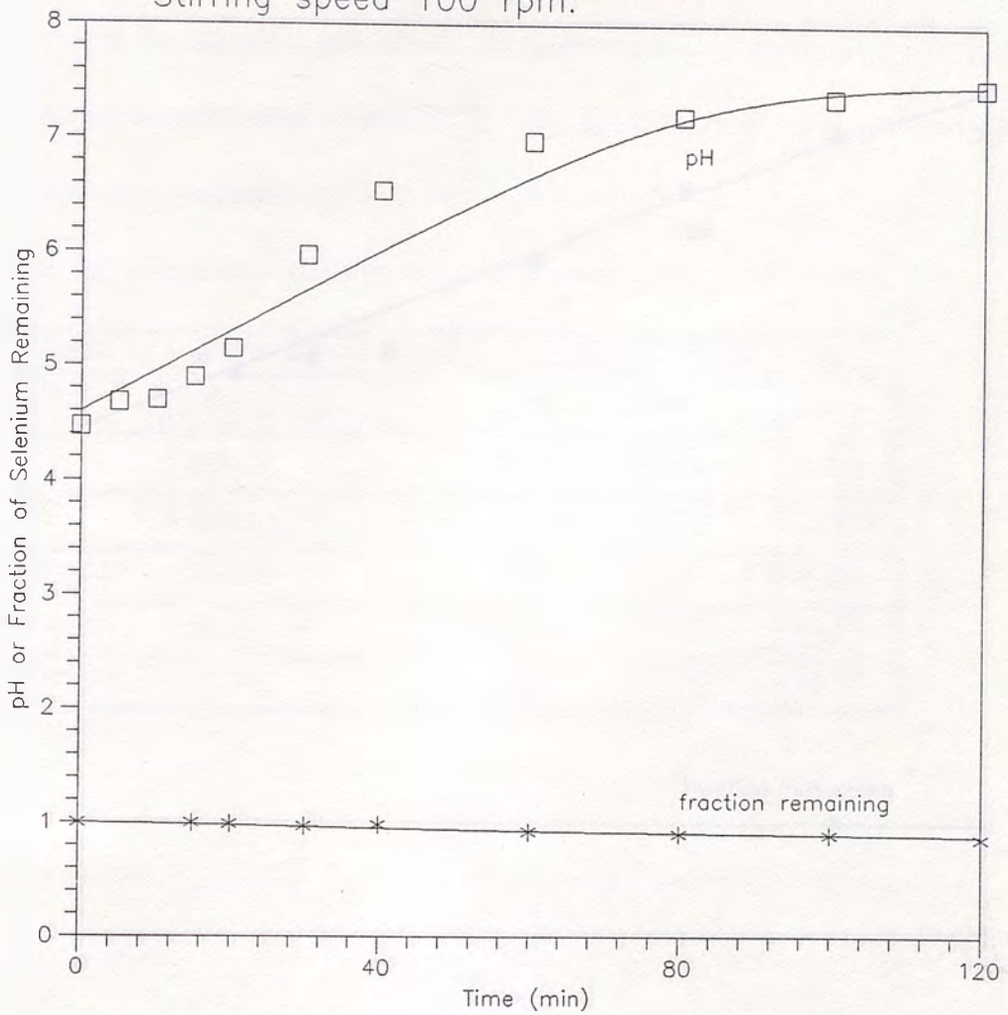

Figure 16: Adsorption of biselenite on alpha–Al_2O_3.
- Temperature 28 degrees celsius.
- Initial concentration 77.61 ppm Se.
- Stirring speed 100 rpm.

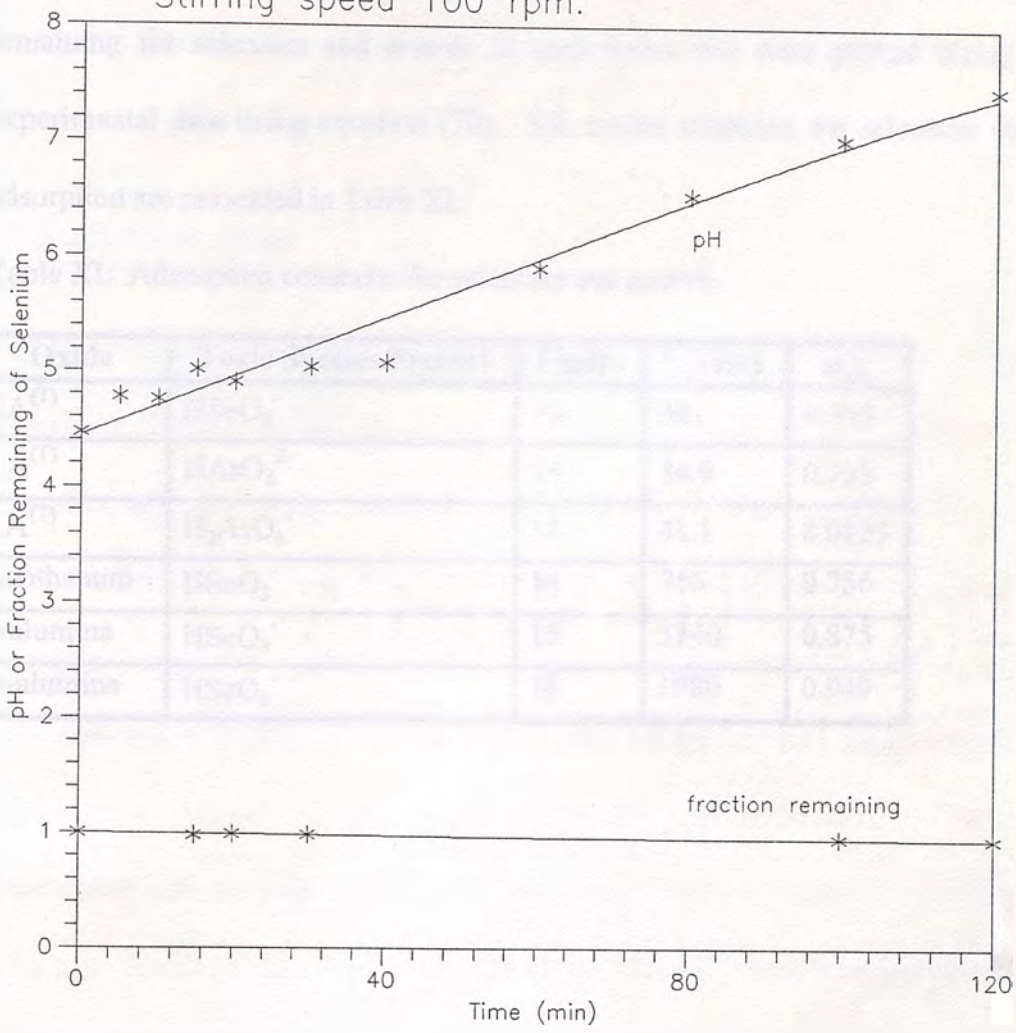

theoretical value of one, given by substituting the charge of the hydrogen ion into equations (63) and (68).

Using the constants in Table X, the time constants for selenium and arsenic in each adsorption test were determined by minimizing the sum of the squares of the residuals between equation (70) and the experimental data. The modeled fraction remaining for selenium and arsenic in each batch test were plotted along with the experimental data using equation (70). The model constants for selenium and arsenic adsorption are presented in Table XI:

Table XI: Adsorption constants for selenium and arsenic.

Oxide	Toxic Species Present	Figure	τ_j (sec)	$\alpha_{j,ss}$
$LA^{(T)}$	$HSeO_3^-$	12	441	0.195
$LA^{(T)}$	$HAsO_4^{2-}$	13	84.9	0.735
$LA^{(T)}$	$H_2AsO_4^-$	13	81.1	0.0125
Lanthanum	$HSeO_3^-$	14	916	0.756
γ-alumina	$HSeO_3^-$	15	3740	0.875
α-alumina	$HSeO_3^-$	16	1980	0.949

The time constants for selenium or arsenic are related to the initial lag in adsorption, where a large time constant correlates with a less rapid initial rate.

From Figures 12 and 13, it is clear that $LA^{(T)}$ is a better adsorbent for biselenite than the arsenic (V) species combined. From Figures 14, 15, and 16, it is evident that lanthanum oxide is the best adsorbent for biselenite, when compared with activated γ-Al_2O_3 and DD-6 at the same initial concentrations. Also, γ-Al_2O_3 worked better than DD-6 from Figures 15 and 16.

iii. Packed Bed Tests:

For tests 1 through 3, in which various combinations of La_2O_3 and activated Al_2O_3 were used to adsorb wastewater sent from ENCYCLE/Texas, the results revealed necessary changes in the experimental method. Problems were encountered with adsorbing and eluting the selenium. These experiments were conducted in percolation mode, which caused channeling in the La_2O_3 and γ-Al_2O_3 sections. Also, the high concentration of heavy metals, such as copper, lead and chromium led to precipitation and consequent fouling of the surface during adsorption and regeneration. During regeneration (elution), instead of the hydroxide ions undergoing an ion exchange mechanism with the adsorbed selenium ions, heavy metal hydroxide precipitates formed, which prevented an effective elution process and blocked liquid flow. In test 3, the effect of increased temperature on regeneration was not fully characterized, but it appeared to give no significant advantage.

In test 4, DD-6 was used to adsorb a low heavy metals content wastewater stream from ENCYCLE/Texas, which contained about 0.1 ppm selenium. The values of selenium mass shown in Table XII were found by numerical integration with the trapezoidal rule for unevenly spaced data points (flowrate is given as superficial velocity or volumetric flowrate divided by the cross-sectional area of the column).[39]

Table XII: Selenium mass balance for test 4.

Stage	Flowrate (m^3/day-m^2)	Se Mass (mg)	Status
Adsorption, 1st cycle	14.0 ± 0.9	1.93	Retained in bed
Elution, 1st cycle	12.0 ± 0.8	0.808	Removed from bed
Activation, 1st cycle	12.0 ± 1.4	1.03	Removed from bed
Adsorption, 2nd cycle	13.7 ± 1.2	0.571	Retained in bed
Elution, 2nd cycle	13.8 ± 1.2	0.391	Retained in bed

The recovery of selenium from adsorption in the first cycle of test 4 was calculated by dividing 1.93 mg Se into 1.838 mg Se (the sum of the selenium removed during elution and activation), to get 95% recovery. Similarly, from the second cycle, the recovery is 0.391 mg Se divided by 0.571 mg Se to give 69% recovery. From inspection of Table XII, it is apparent that the elution stage was not able to recover all the selenium in the first or second cycles. This was because the column was not saturated with enough selenium to provide a large driving force for selenium desorption upon elution with NaOH. A maximum of 95% recovery, combined with a low concentration factor (ratio of the volume of wastewater treated to the volume of eluant), indicated that improvements in the processing method were required. Ideally, recovery should be nearly 100%, and the concentration factor should be greater than 10 for industrial purposes. In this test, there

was not enough wastewater available to saturate the column, which explains why elution was not more effective. Also, the percent relative standard deviation (%RSD) for the selenium analysis was greater than 50%, which, combined with the trapezoidal integration technique, may have caused error in the calculations.

Tests 5 and 6 were designed to determine the ultimate capacity of DD-6 and γ-Al_2O_3 for selenium, and to find the number of cycles the adsorbents would remain effective. From this information, the best alumina can be determined and used to make a mixed oxide incorporating La_2O_3. These tests were run simultaneously, with the same influent solutions and flowrates. In this thesis, only results from the first cycle are presented. Figures 17 and 18 show the breakthrough curves for tests 5 and 6, γ-Al_2O_3 and DD-6, respectively. In both columns, the selenium concentration was less than 0.2 ppm until about 350 L was treated. Figures 19 and 20 show the elution curves for tests 5 and 6, which follow an exponential-type pattern. From Figures 17 through 20, and other information combined, the loading of selenium onto the oxides and the amount of selenium eluted was determined and is presented in Table XIII:

Table XIII: Selenium capacity and elution effectiveness for tests 5 and 6.

Test	Selenium Adsorbed (gr)	Selenium Loading (mg Se/gr)	Selenium Eluted (gr)	% Recovery
5, γ-Al_2O_3	51	37	47	92
6, DD-6	61	59	61	100

From Table XIII, it is clear that DD-6 has a higher capacity for selenium, and that it is eluted with greater effectiveness than γ-Al_2O_3. A major advantage of using γ-Al_2O_3

Figure 17: Test 5, packed bed adsorption of selenium with activated gamma-Al_2O_3.
- Inlet concentration: 86.9 +/- 7.1 ppm Se.
- Flow: 11.6 +/- 1.7 m^3/day-m^2, downflow.

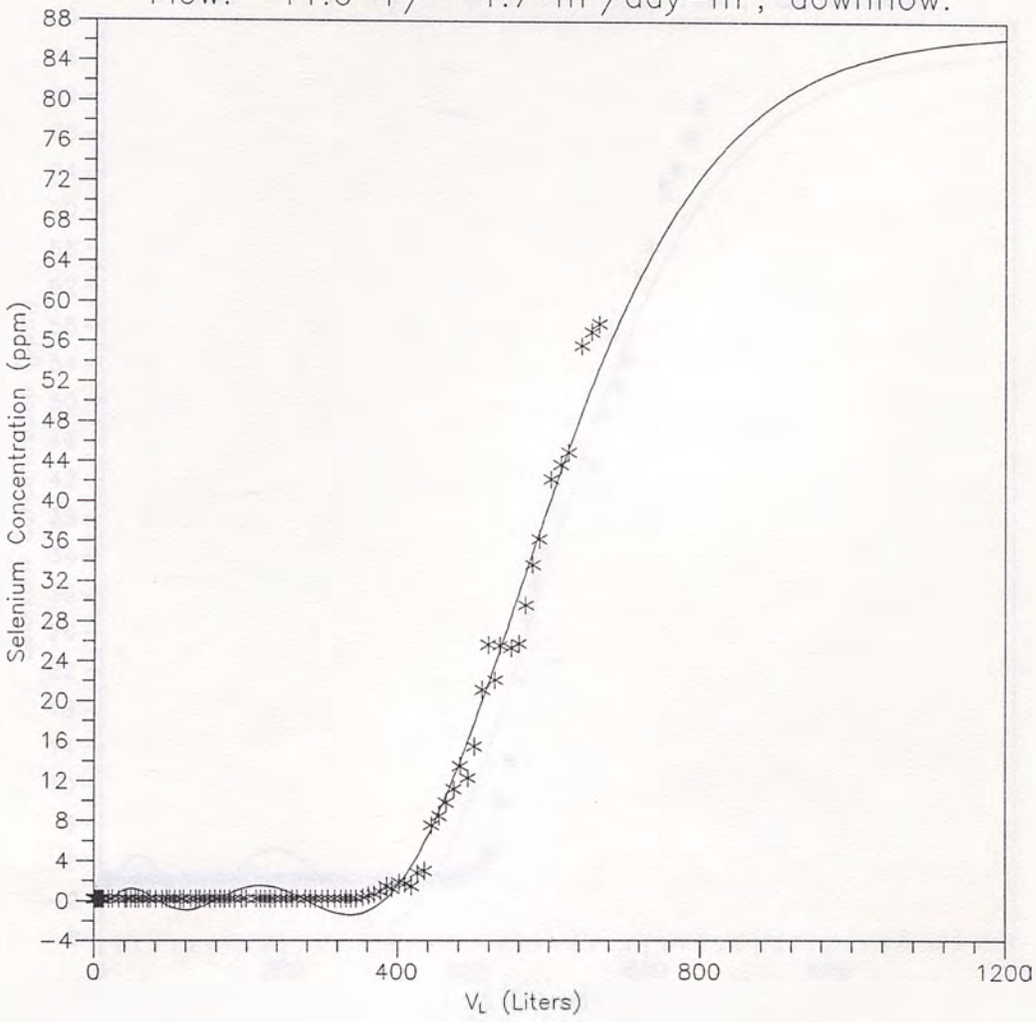

Figure 18: Test 6, packed bed adsorption of selenium with DD-6.
- Inlet concentration: 86.9 +/- 7.1 ppm Se.
- Flow: 11.4 +/- 0.6 $m^3/day-m^2$, downflow.

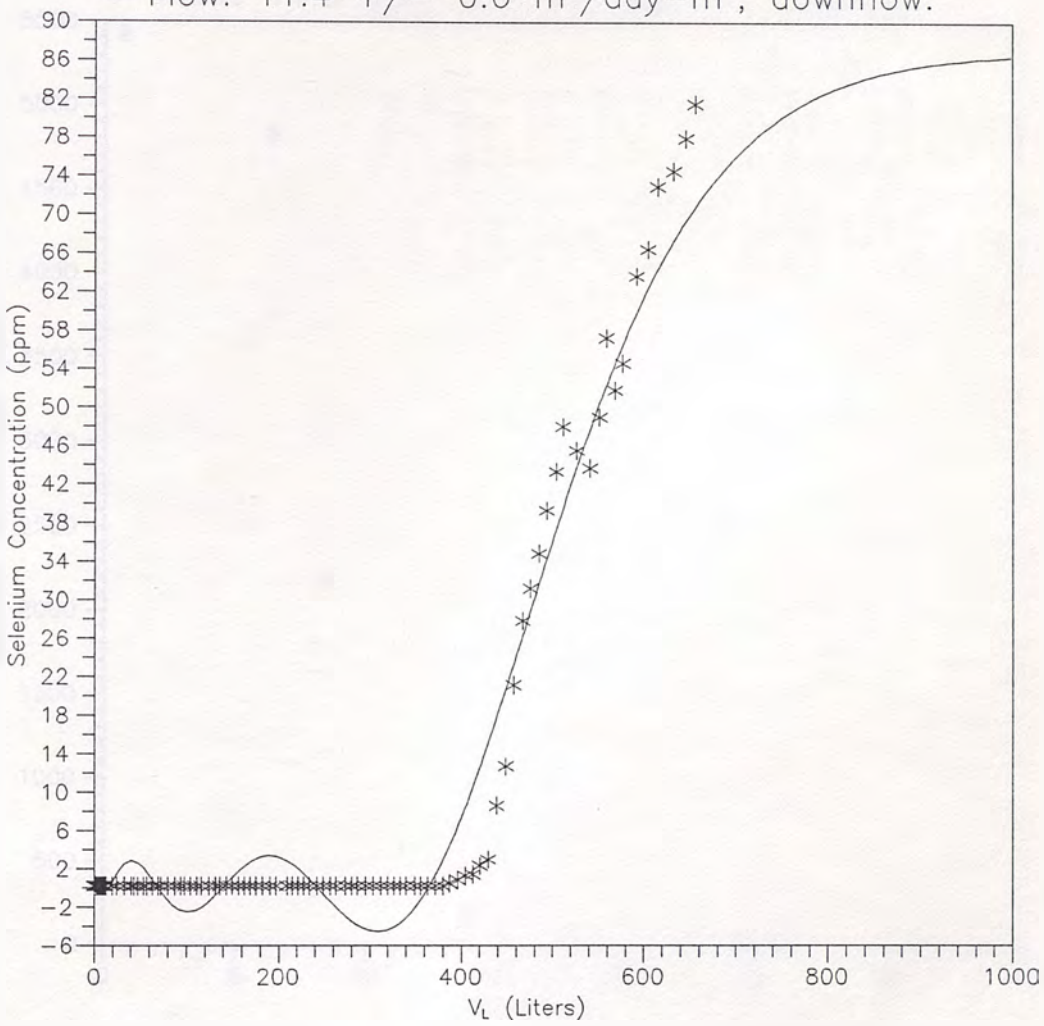

Figure 19: Test 5, elution of selenium with sodium hydroxide from activated gamma-Al_2O_3.
- Inlet pH: 13.53 +/- .05.
- Flow: 11.6 +/- 1.7 $m^3/day-m^2$, downflow.

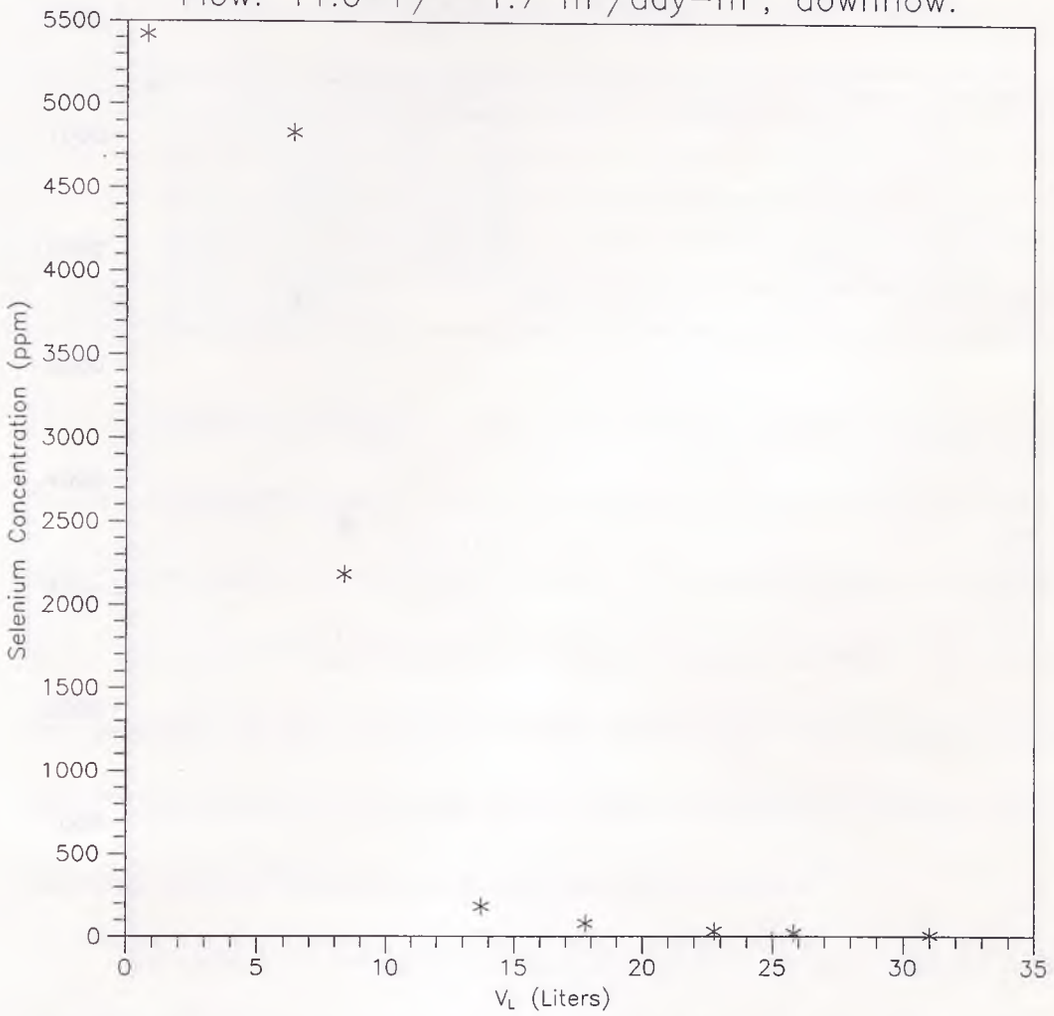

Figure 20: Test 6, elution of selenium with sodium hydroxide from DD-6.
- Inlet pH: 13.53 +/- .05.
- Flow: 11.4 +/- .1 $m^3/day-m^2$, downflow.

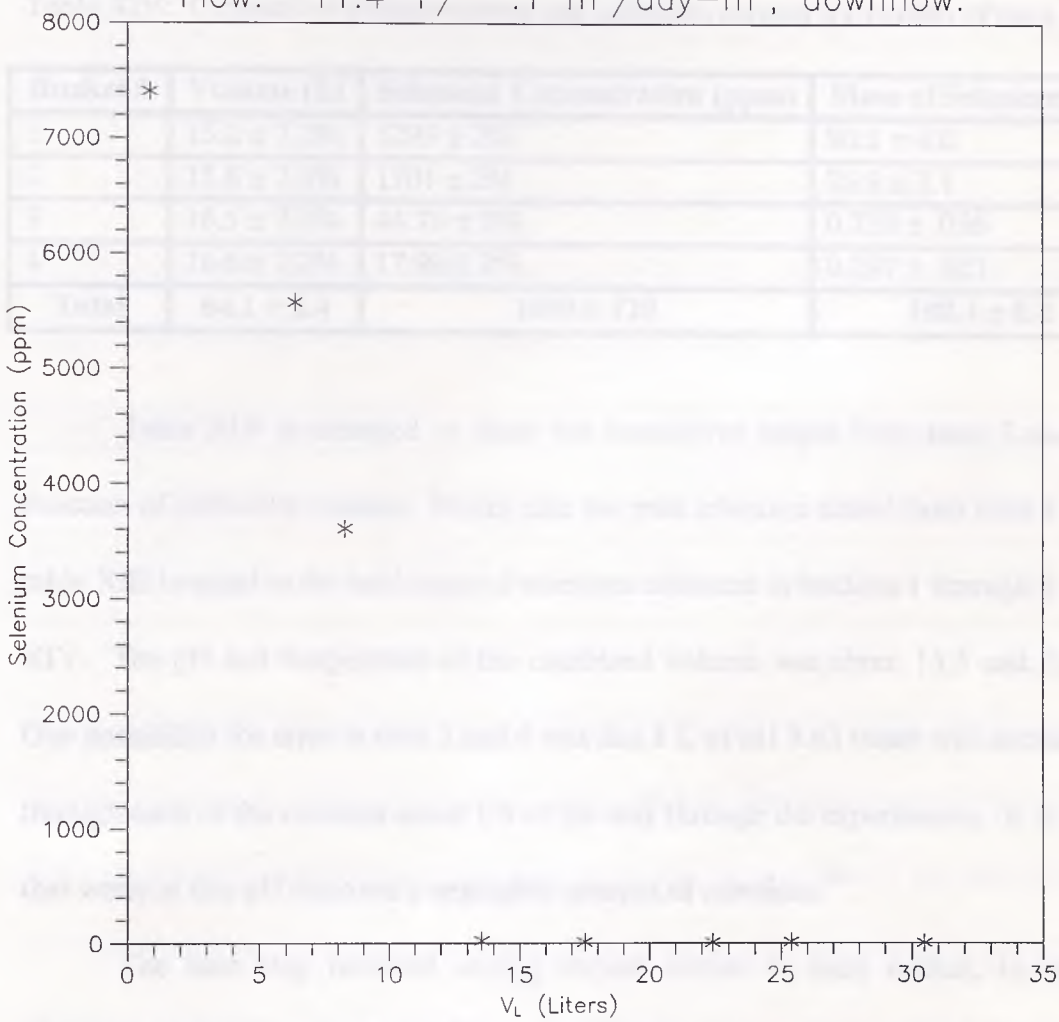

or DD-6 to adsorb selenium is illustrated in Table XIV, where it is evident that the total elution volume for tests 5 and 6 combined is only 64.1 ± 2.4 L, which corresponds to a concentration factor of about 11, if only the volume is counted during the period when the selenium concentration was less than 0.2 ppm (Figures 17 and 18).

Table XIV: Cumulative elution volume and selenium content for elution of tests 5 and 6.

Bucket #	Volume (L)	Selenium Concentration (ppm)	Mass of Selenium (gr)
1	15.2 ± 7.2%	5295 ± 2%	80.5 ± 6.0
2	15.8 ± 7.6%	1701 ± 2%	26.9 ± 2.1
3	16.5 ± 7.3%	44.70 ± 2%	0.738 ± .056
4	16.6 ± 7.2%	17.90 ± 2%	0.297 ± .023
Total	**64.1 ± 2.4**	**1690 ± 120**	**108.4 ± 6.4**

Table XIV is arranged to show the cumulative output from tests 3 and 4 as a function of collection buckets. Notice that the total selenium eluted from tests 5 and 6 in table XIII is equal to the total mass of selenium collected in buckets 1 through 4 in Table XIV. The pH and temperature of the combined volume was about 13.5 and 23 ± 1°C. One possibility for error in tests 5 and 6 was that 8 L of pH 9.63 water was accidently run through each of the columns about 1/8 of the way through the experiments. It is believed that water at this pH removed a negligible amount of selenium.[26]

The next step involved adding ferrous sulfate to each bucket, to cause the reduction of oxyanions of Se(IV) to elemental selenium. The first bucket was also supplied with 277 gr of NaOH. Table XV shows the outcome of this recovery method:

Table XV: Reduction of elution effluent from tests 5 and 6 to elemental selenium.

Bucket #	$FeSO_4$ Added (gr)	Selenium Concentration After 24 Hours (ppm)	wt % Se Removed
1	770	2011 ± 2%	62
2	261	1244 ± 2%	27
3	7.16	no change	0
4	2.89	no change	0

As was expected, the reduction/precipitation effectiveness decreased with decreasing selenium concentration.

Following elution of tests 5 and 6 with sodium hydroxide, HCl was used to reactivate the column. The results of activation for tests 5 and 6 are given in Table XVI:

Table XVI: Activation of tests 5 and 6 following elution.

Test	Volume Used (L)	pH	Selenium Concentration (ppm)
5	5.22	1.55	0.629 ± 2%
	7.35	not measured	1.051 ± 2%
6	5.30	1.99	< 0.2
	7.47	1.42	< 0.2

Table XVI shows that significant amounts of selenium were being carried out of the column from test 5 during activation. This agrees with the elution results shown in Table XIII, since test 5 had 8% of the adsorbed selenium remaining in it, and test 6 had none. The total volume and selenium concentration from the activation of tests 5 and 6 combined was about 16.6 L and 9.45 ± 2% ppm Se.

The packed bed modeling results for tests 5 and 6 are shown on Figures 17 and 18 as solid lines. The modeled curves were calculated from equation (81), with the best fit constants determined by the SAS (procedure TNLIN) statistical curve fitting software for

nonlinear equations. The values of λ_j found by SAS were readily converted to k_j with the known flowrates, specific surface areas and solids concentrations, via equation (78). Table XVII lists the information extracted from the packed bed modeling results.

Table XVII: Packed bed modeling results for selenium as biselenite.

Selenium Constants	Test 5 (activated γ-Al_2O_3)	Test 6 (DD-6)
k_{Se} (nm/hr)	0.030	0.049
c_{1Se} (no units)	-0.9900	-0.9823
c_{2Se} (m^{-3})	-16.35	-23.56
c_{3Se} (m^{-6})	65.13	329.2
c_{4Se} (m^{-9})	-3,096	-10,340
c_{5Se} (m^{-12})	15,570	65,960
c_{6Se} (m^{-15})	-42,230	-185,200

Several aspects of the modeled results are encouraging. First, the mass transfer coefficients due to the concentration and potential gradients were readily calculated from the value of λ_{Se} found by SAS. Although there is no literature data with which to compare these values, the fact that the k_{Se} coefficient for test 6 with DD-6 is larger than the coefficient for test 5 with activated γ-Al_2O_3 agrees with the result found earlier that DD-6 adsorbed more selenium than activated γ-Al_2O_3. Furthermore, DD-6 has a smaller average particle size than activated γ-Al_2O_3, which is known to lead to greater mass transfer coefficients in other systems. Another encouraging aspect of the model is that it fits the experimental data reasonably well. The main deviation between the model and the experimental data for test 5 (Figure (17)) occurs while the selenium concentration is

below 0.2 ppm, during which time oscillations arise. The oscillations are more dramatic for test 6 (Figure (18)), and the breakpoint was partly missed.

VIII. Discussion:

i. Electrokinetic Measurements:

The IEP measurements on activated γ-Al_2O_3 and La_2O_3 showed the upward shift in pH_{zpc} that occurs when sulfate ions are present. Due to the similarities in chemistry between sulfate and selenate, a similar phenomenon should occur in the presence of selenate. The upward shift in pH_{zpc} may lead to increased adsorption rates and capacity, due to greater coulombic attraction. Furthermore, this phenomenon indicates that chemisorption is the removal mechanism for oxy-anions of selenium.[15,28]

ii. Batch Tests:

In order to emphasize the importance of a transport model, a method for making the batch model fully predictive is demonstrated below. Essentially, an empirical method of finding the time constants for hydrogen, selenium and arsenic, and the fraction remaining at steady state of selenium and arsenic, was developed. However, it is important to note that more data is required to make the model statistically valid. From equations (61) through (65) and (71), the time constant for selenium or arsenic adsorption should have the following functionality:

$$\tau_j = \Phi\left(D_j, pH_{zpc}, pH_o, r_{Hj}, r_{ej}, A_{sp}C_s, N_{Re}, D_p\right) \tag{91}$$

From dimensional analysis, the following empirical equation was developed:

$$\tau_j = D_j^{-1} pH_{zpc}^{a} r_{Hj}^{b} r_{ej}^{c} pH_o^{d} \left(A_{sp}C_s\right)^{e} N_{Re}^{f} D_p^{2-b-c+e} \tag{92}$$

The exponents to equation (92) are given on Figure 21, from which it is clear that there is a one to one relationship between the experimentally determined selenium and arsenic adsorption time constants and the ones predicted from equation (92). Any set of consistent units may be used with equation (92).

The empirical equation for the hydrogen ion time constant is a dimensional equation, with the hydrated and effective radii in equation (92) replaced with temperature and viscosity as follows:

$$\tau_{H^+} = D_{H^+}^{-1} pH_{zpc}^{a} T^{b} u^{c} pH_{o}^{d} \left(A_{sp} C_{s}\right)^{e} N_{Re}^{f} D_{p}^{2-b-c+e} \tag{93}$$

S.I. units (m, kg, s, °K) must be used with equation (93). The exponents are given on Figure 22, where a one to one relationship exists between the experimentally determined hydrogen ion time constants and the ones found from equation (93).

An empirical equation for the fraction remaining of selenium or arsenic at steady state is a dimensional equation, with the hydrated radius in equation (92) replaced with the initial concentration as follows:

$$\alpha_{j,ss} = D_{j}^{-1} pH_{zpc}^{a} C_{o,j}^{b} r_{ej}^{c} pH_{o}^{d} \left(A_{sp} C_{s}\right)^{e} N_{Re}^{f} D_{p}^{2-b-c+e} \tag{94}$$

S.I. units (m, kg, s) must be used with equation (94), except for the initial concentration, which must have units as follows: mg toxic element in species per liter. For instance, with selenium, the units of concentration are milligrams of selenium as biselenite per liter. The exponents are given on Figure 23, where a one to one relationship exists between the experimentally determined fraction remaining of selenium or arsenic at steady state, and the ones found from equation (94).

Figure 21: Experimental versus empirical time constants for arsenic and selenium adsorption.
- Use S.I.; meters, Kg, sec units.
- a=8.378; b=12.91; c=-10.79; d=-.075;
- e=-.477; f=1.27; g=-.594.

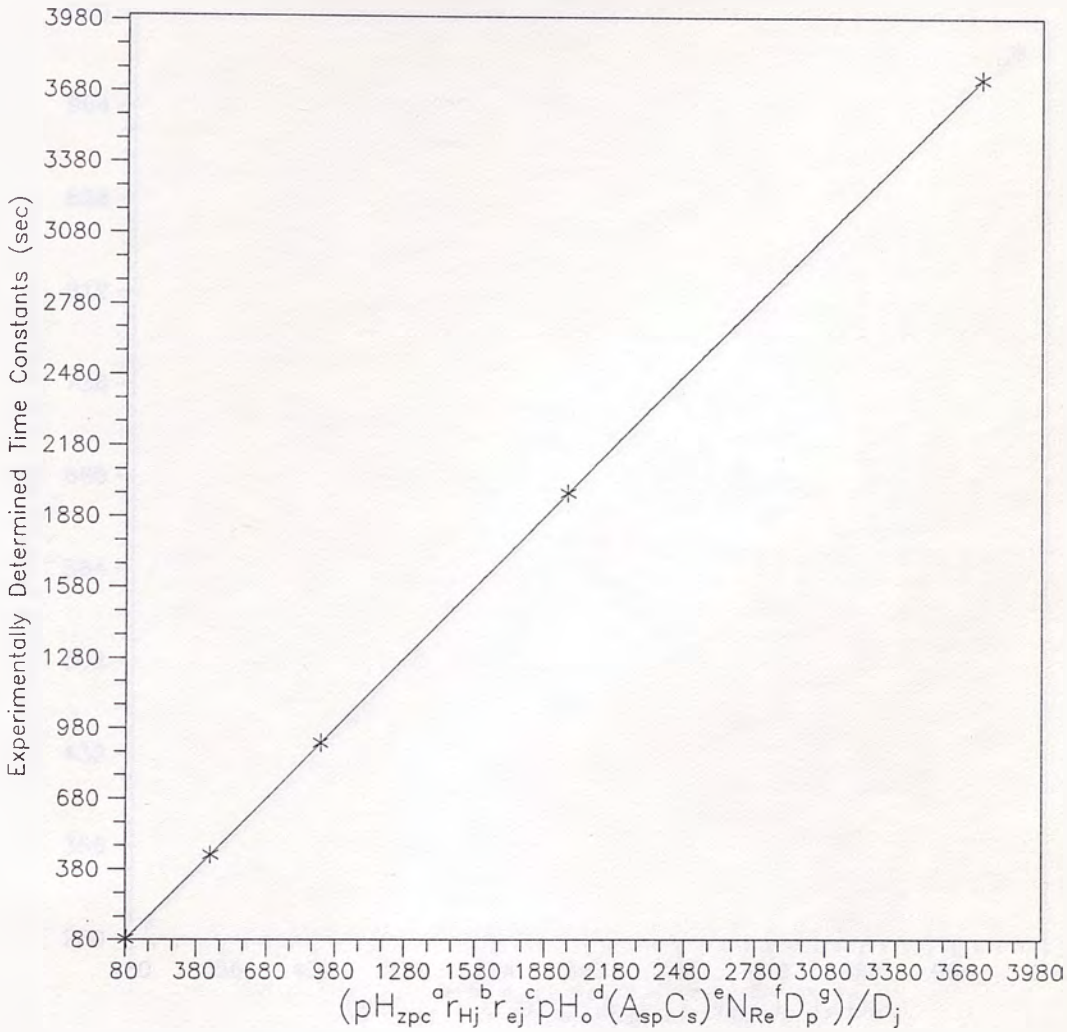

Figure 22: Experimental versus empirical time constants for pH dynamics.
- Use S.I.; meters, Kg, sec, Kelvin units.
- a=−1.167; b=−.4557; c=4.309; d=.5802;
- e=.8265; f=.5992; g=−1.027.

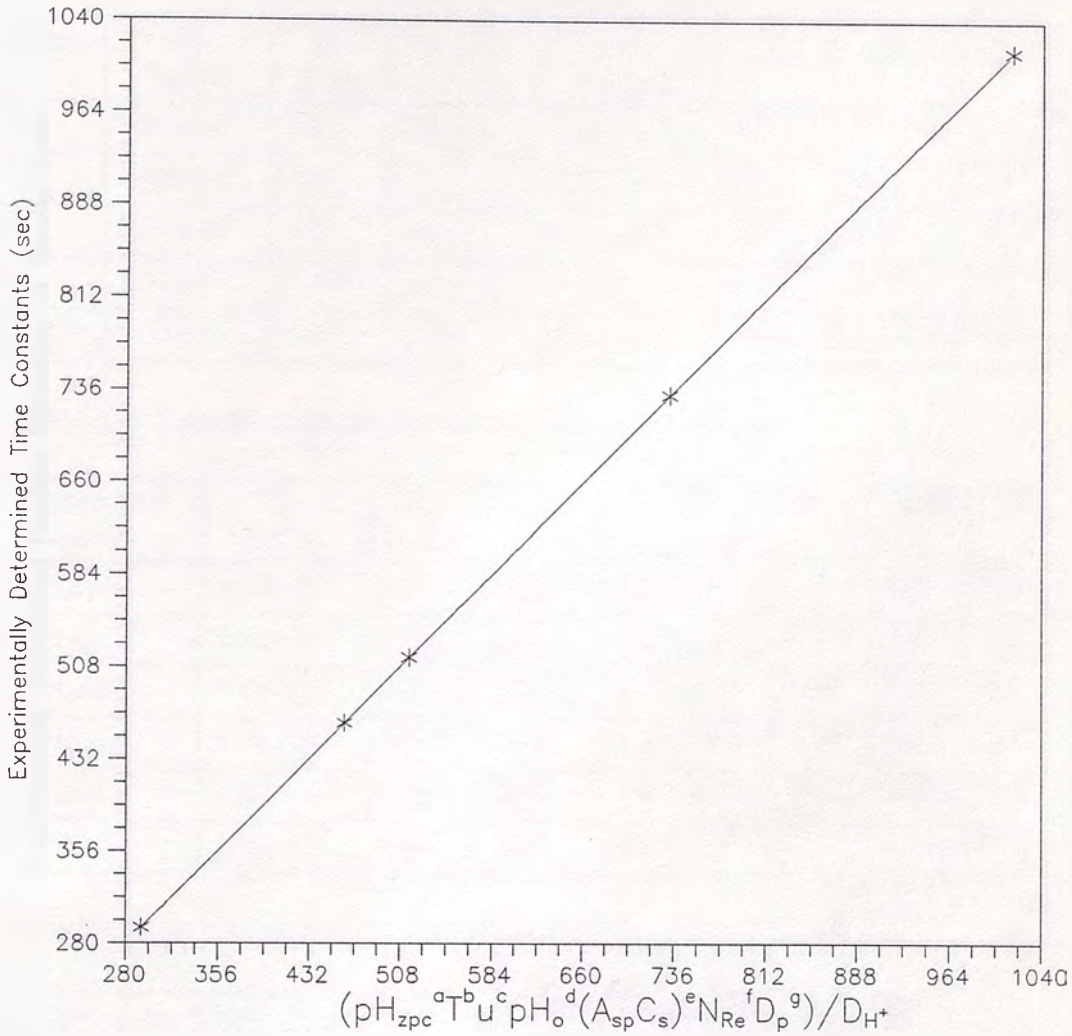

Figure 23: Experimental versus empirical fraction remaining at steady state for selenium and arsenic.
- Use meters, Kg, sec units except for C_{oj}.
- C_{oj} has units of mg of element/L of solution.
- a=−58.1; b=2.079; c=−9.420; d=6.388;
- e=−4.513; f=−3.189; g=4.828.

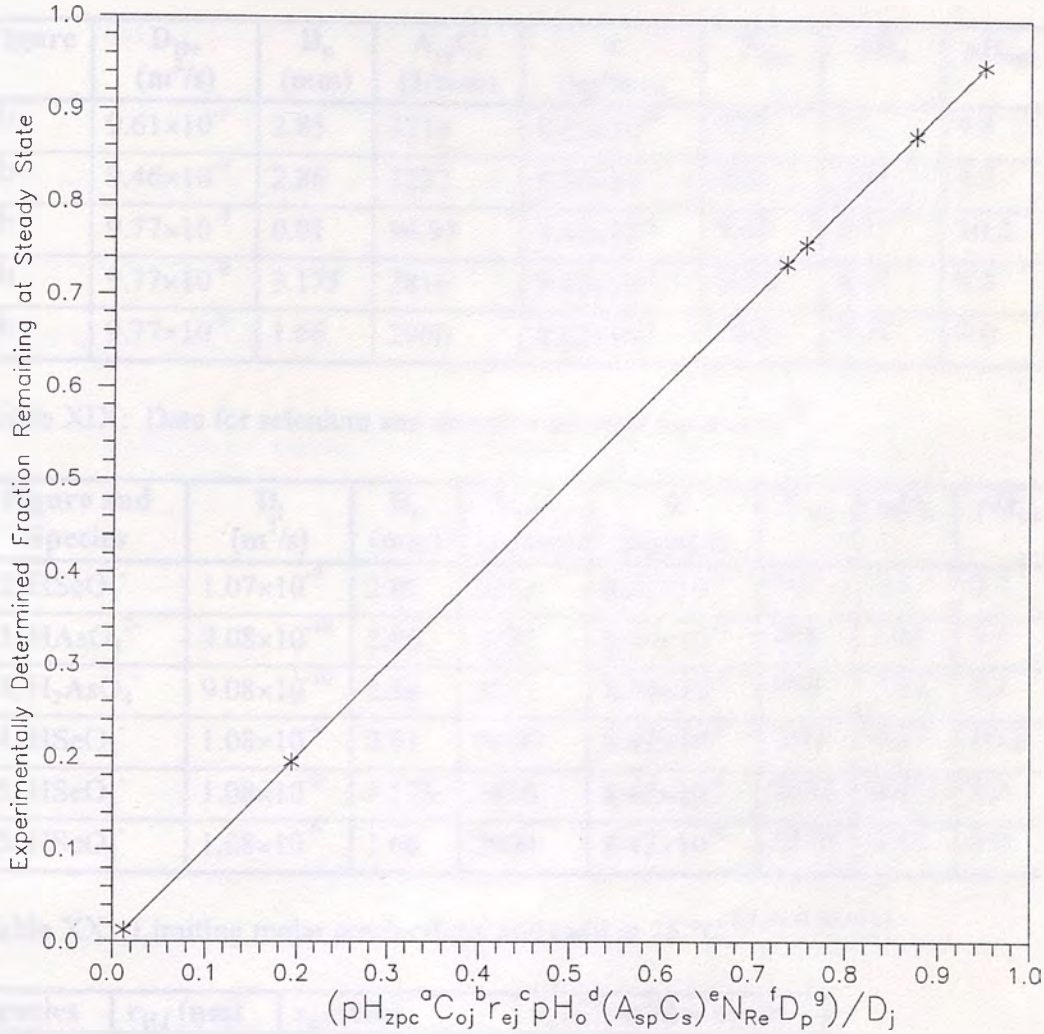

The exponents in equations (92) through (94) were found by minimizing the sum of the residuals squared between the equations and the experimental data. The data used for fitting these equations are given in the tables below.

Table XVIII: Data for hydrogen ion empirical time constant equation.[26]

Figure	D_{H+} (m^2/s)	D_p (mm)	$A_{sp}C_s$ (1/mm)	u (kg/m-s)	N_{Re}	pH_o	pH_{zpc}
2b	9.61×10^{-9}	2.85	3218	8.62×10^{-4}	507	3.3	9.3
3b	9.46×10^{-9}	2.86	3232	8.74×10^{-4}	498	7.81	9.3
4b	9.77×10^{-9}	0.01	94.97	8.42×10^{-4}	9.48	4.47	10.2
5b	9.77×10^{-9}	3.175	2816	8.42×10^{-4}	3010	4.47	9.2
6b	9.77×10^{-9}	1.66	2900	8.42×10^{-4}	1570	4.47	9.0

Table XIX: Data for selenium and arsenic empirical equations.[26]

Figure and Species	D_j (m^2/s)	D_p (mm)	$A_{sp}C_s$ (1/mm)	u (kg/m-s)	N_{Re}	pH_o	pH_{zpc}
12, $HSeO_3^-$	1.07×10^{-9}	2.85	3218	8.62×10^{-4}	507	3.3	9.3
13, $HAsO_4^{2-}$	9.08×10^{-10}	2.86	3232	8.74×10^{-4}	498	7.81	9.3
13, $H_2AsO_4^-$	9.08×10^{-10}	2.86	3232	8.74×10^{-4}	498	7.81	9.3
14, $HSeO_3^-$	1.08×10^{-9}	0.01	94.97	8.42×10^{-4}	9.48	4.47	10.2
15, $HSeO_3^-$	1.08×10^{-9}	3.175	2816	8.42×10^{-4}	3010	4.47	9.2
16, $HSeO_3^-$	1.08×10^{-9}	1.66	2900	8.42×10^{-4}	1570	4.47	9.0

Table XX: Limiting molar conductivity and radii at 25 °C.[2,4,34,41,42,43,44]

Species	$r_{H,j}$ (nm)	$r_{e,j}$ (nm)	ν_j (C^2-m^2/J-s-mole)
$HSeO_3^-$	0.45	0.211	40×10^{-4}
$HAsO_4^{2-}$	0.45	0.248	136×10^{-4}
$H_2AsO_4^-$	0.45	0.248	34×10^{-4}
H^+	0.90	not determined	349.65×10^{-4}

The diffusion coefficients were determined from the following formula:[34]

$$D_j = \frac{RT\nu_j}{F^2 z_j^2} \tag{95}$$

The molar conductivity of the hydrogen ion at 50 °C (462.3 $\times 10^{-4}$ C^2-m^2/J-s-mole) was used to estimate the molar conductivity at higher temperatures by linear interpolation.[42] One advantage of using empirical equations is that the effective diffusion coefficients need not be known, and the radii of the adsorbed ions can be assumed to equal their crystallographic radii. Any non-idealities will be taken into account by the empirical nature of the equations.

The Reynolds number was determined by the following formula in Tables XVIII and XIX:

$$N_{Re} = \frac{\rho V_o D_p}{u} \tag{96}$$

The velocity used in equation (96) was found by employing two methods. In the case where stirring was adjusted to the onset of a vortex, the velocity was taken as the terminal velocity of the particles. When the stirring speed was 100 rpm, the velocity was taken as two times the radial velocity.

iii. Packed Bed Tests:

The concentrated selenium solution obtained from elution of the saturated columns of tests 5 and 6 were precipitated as elemental selenium by the addition of

ferrous sulfate. The mechanism is probably a combination of two oxidation-reduction reactions shown below, following the formation of ferrous hydroxide:

$$FeSO_{4(s)} + 2NaOH_{(aq)} \rightarrow Fe(OH)_{2(s)} + Na_2SO_{4(aq)} \quad (97)$$

$$Na_2SeO_{3(aq)} + 4Fe(OH)_{2(s)} \rightarrow 2Fe_2O_{3(s)} + Se_{(s)} + 3H_2O_{(l)} + 2NaOH_{(aq)} \quad (98)$$

$$Na_2SeO_{3(aq)} + 6Fe(OH)_{2(s)} \rightarrow 2Fe_3O_{4(s)} + Se_{(s)} + 5H_2O_{(l)} + 2NaOH_{(aq)} \quad (99)$$

The standard state free energy of reactions (98) and (99) are -45.7 Kcal/mole and -57.0 Kcal/mole, respectively. This suggests that without kinetic limitations, reaction (99) is the predominant route to elemental selenium. The predominant formation of magnetite, along with elemental selenium (equation (99)), concurs with previous workers' findings.[45] According to this mechanism, about 16% less than the stoichiometric amount of $FeSO_4$ required was added to the effluent from tests 5 and 6, which partly explains the low selenium precipitation efficiency.

Figure 24 shows the concentration as a function of bed length for test 5 during breakthrough. From Figures 17, 18 and 24, it is clear that the concentration in the column and, hence, the degree of saturation of the adsorbent, is a function of volume treated and bed length. It is also apparent that the entire bed had nearly reached its maximum saturation at the time this profile was taken. This condition was desirable and is an important aspect of wastewater treatment design and cost estimation because it is necessary to use the entire bed of adsorbent efficiently.

The packed bed modeling results obtained thus far limit its predictive nature to concentration as a function of volume treated. From the modeled values of c_{1Se} through

Figure 24: Test 5, concentration versus length for adsorption of selenium with gamma–Al_2O_3. – V_L = 665 L.

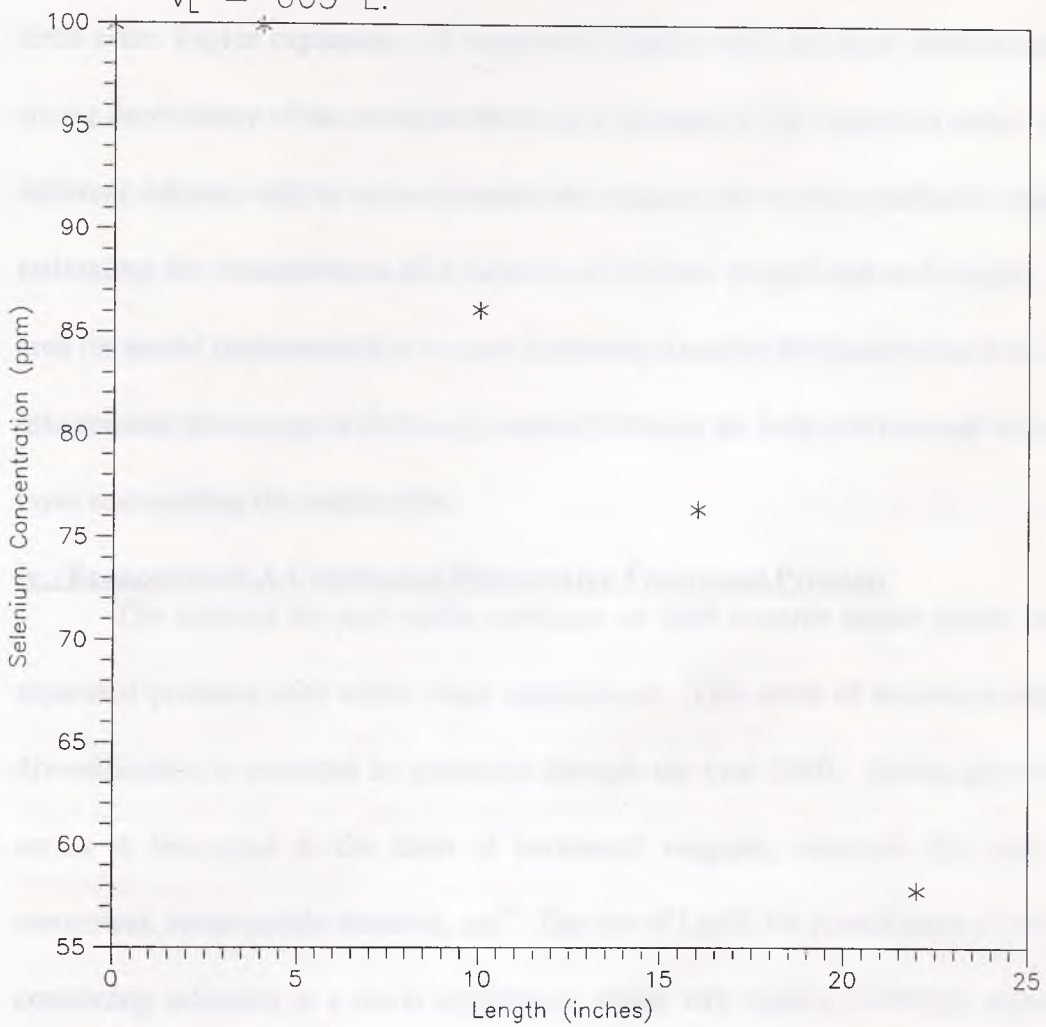

c_{6Se}, one set of mass transfer coefficients could not be arrived at for predicting the values of c_{1Se} through c_{6Se} at different bed lengths. However, the modeled c_{1Se} constants, which are about -1 in Table XVII, agree with the initial condition that must be satisfied and the model also satisfies the steady state condition at complete bed saturation.

One cause of the model inconsistencies may be the approximation made by the sixth order Taylor expansion. A sensitivity analysis with the SAS software revealed a strong dependency of the modeled results as a function of the expansion order. Perhaps a different solution will be more accurate and enhance the models predictive capability at estimating the concentration as a function of volume treated and bed height. Another area for model improvement is to more accurately describe the desolvation flux, by taking into account the change in dielectric constant between the bulk solution and the molecular layer surrounding the metal oxide.

iv. Economics of A Continuous Wastewater Treatment Process:

The demand for rare earths continues to shift towards higher purity mixed and separated products with wider range applications. This trend of increased demand and diversification is expected to accelerate through the year 2000. Strong growth for rare earths is forecasted in the areas of permanent magnets, materials for auto catalytic converters, rechargeable batteries, etc.[6] The use of La_2O_3 for remediation of wastewaters containing selenium is a novel application which will require relatively impure La_2O_3 (99.9%). Ultimately, La_2O_3 will be combined with activated Al_2O_3 to create a high surface area, insoluble adsorbent for oxy-anions of selenium at low concentrations

(presumably, 10% La_2O_3 and 90% Al_2O_3). Target industries include mining, petroleum refining, agricultural, and inorganic wastewater treatment, to name a few.

A typical wastewater stream from ENCYCLE/Texas is 0.5 MGD, and contains 1 ppm selenium. The four cylindrical packed beds chosen for this order of magnitude economic estimate each have a length of 5 meters and a diameter of 0.5 meters (this is based on L/D = 10, to avoid end effects). The major costs considered were labor, capital investment for installation of the packed beds, reagent costs, and adsorbent costs. The labor cost is based on the assumption that one dedicated maintenance operator can run the system 24 hr/day for $14/hr. The capital investment includes the cost of the packed beds, including installation and auxiliaries.[40] The cost was amortized over ten years by the straight line method, assuming a salvage value of 1/5 the initial investment Reagent costs include NaOH for elution and HCl for activation. The adsorbent cost depends upon how many cycles the sorbent remains effective.

Two adsorbents were considered for this estimate: DD-6/10% La_2O_3 and activated γ-Al_2O_3/10 % La_2O_3. Price data obtained for the three adsorbents are from the bulk producers and only apply to applications requiring several tons. The cost of the mixed oxide combinations were calculated from the mass percentages. The lowest cost La_2O_3 is $6.35/lb, 99.9% pure, and obtained from China through ProChem. DD-6 ($0.65/lb) and activated γ-Al_2O_3 ($0.683/lb) are both produced by ALCOA. The ultimate capacities of the two adsorbents were assumed to equal that of their alumina base

component, found from Table XIII. The addition of La_2O_3 is expected to remove selenium to lower concentrations than the activated aluminas alone.

Figure 25 shows the outcome of the wastewater treatment cost estimate, which ranged between 1 and 2 cents/gal, depending on the number of cycles. The largest contributors to the total treatment cost per gallon were reagents and adsorbents. According to Figure 25, the DD-6/10% La_2O_3 combination is the cheapest overall, except at 10 cycles, where the two adsorbents considered are equal in cost. However, recent experiments showed that activated γ-Al_2O_3 does not remain insoluble during the extreme pH conditions of cyclic treatment and therefore will not last 10 cycles.[26] On the other hand, DD-6 retained its surface morphology and remained insoluble after one cycle in test 6. Other differences between the two adsorbents are the adsorbent costs and bulk densities. Although activated γ-Al_2O_3 is more expensive, it is also more dense, which means it requires less packed bed volume per unit mass.

Figure 25: Wastewater treatment cost based on 0.5 MGD and 1 ppm Se influent.

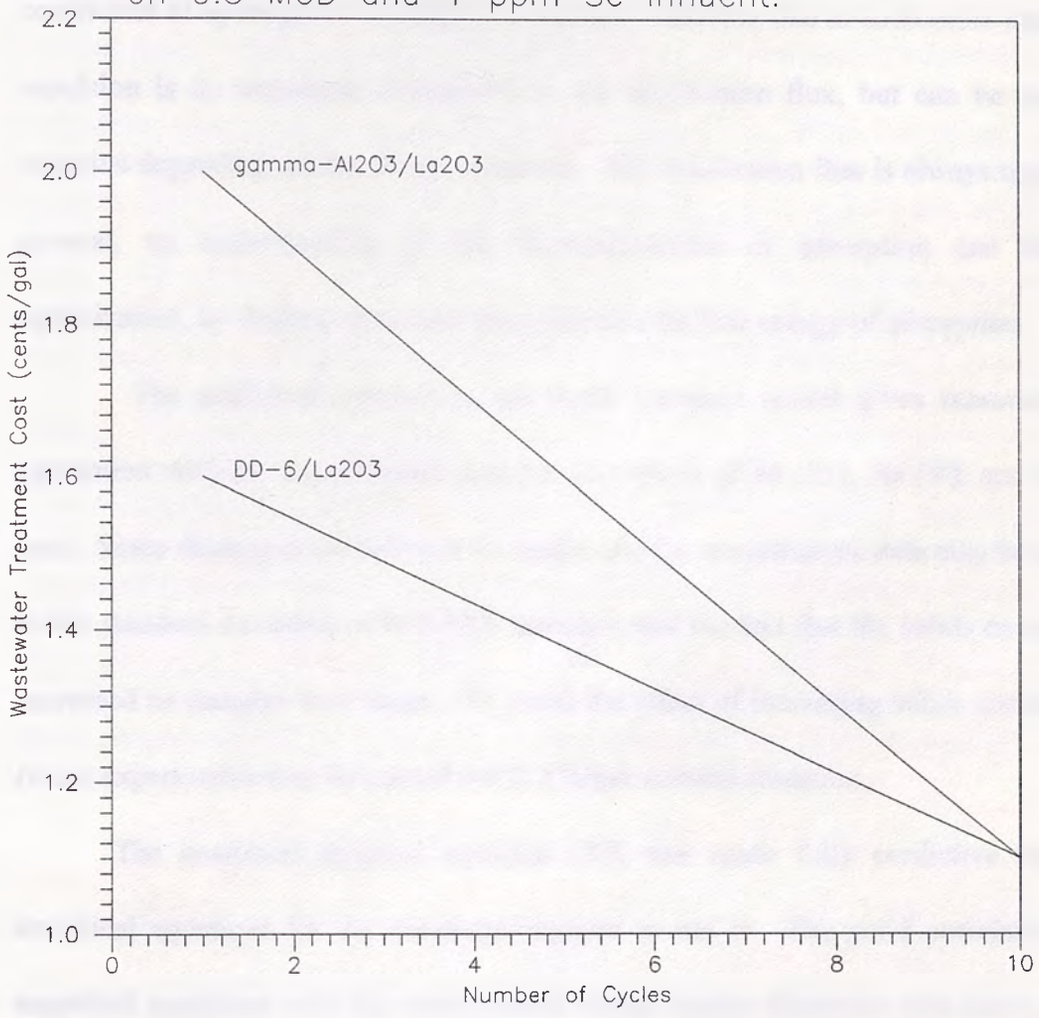

IX. Conclusions:

The transport of ions to the La_2O_3 and activated Al_2O_3 surfaces is a function of three fluxes: diffusion, coulombic attraction (or repulsion), and desolvation. Initially, the diffusion flux is the largest flux, which explains the rapid uptake of hydrogen ions by the metal oxides that is always observed experimentally. In particular, the diffusion coefficient of hydrogen is the largest of any ion. The flux due to coulombic attraction or repulsion is in magnitude comparable to the desolvation flux, but can be positive or negative depending on the charge of the ion. The desolvation flux is always negative. In general, an understanding of the thermodynamics of adsorption can help with optimization, by finding conditions that minimize the free energy of adsorption.

The analytical solution to the batch transport model gives reasonably good agreement with the experimental data for adsorption of Se (IV), As (V), and hydrogen ions. Some discrepancies between the model and the experimental data may be attributed to the standard deviation of ICP-AES detection and the fact that the solids concentration increased as samples were taken. To avoid the effect of increasing solids concentration, future experiments may be carried out in a larger volume container.

The analytical solution, equation (70), was made fully predictive by finding empirical equations for the constants required to use it. The good correlation of the empirical equations with the experimental values further illustrates that three gradients exist between the bulk solution and the oxide-water interface: concentration, potential, and ionic size. Furthermore, it is clear that the pH_{zpc} and the initial pH of the solution have an effect on the kinetics and extent of adsorption. The high pH_{zpc} of La_2O_3 explains

why it is a better adsorbent for biselenite than activated γ-Al_2O_3 or DD-6, even though the aluminas had much higher surface areas. This reasoning may also explain why γ-Al_2O_3 is a better adsorbent for biselenite than DD-6.

From the packed bed tests conducted thus far, it is know that the NaOH eluant must be in the range of pH 13.5 to remove selenium with high efficiency; that the mode of flow should be plug flow; that the degree of selenium saturation or loading effects the efficiency of selenium removal by NaOH elution; that DD-6 has a higher loading capacity than activated γ-Al_2O_3 (59 mg Se(IV)/gr compared with 37 mg Se(IV)/gr); that DD-6 is eluted with better efficiency than activated γ-Al_2O_3; and that wastewaters with high heavy metal concentrations dictate that a different eluant/activation reagent/cycle be found. The last result has major implications for the mining industry in general, and ENCYCLE/Texas in particular. We also found that DD-6 remained essentially insoluble compared with activated γ-Al_2O_3 after one complete cycle of treatment in tests 5 and 6. The cyclic potential of DD-6 combined with the economic estimate of Figure 25 suggests that it may be the best Al_2O_3 base compound for a mixed oxide containing La_2O_3.

X. Recommendations:

Although the ability of La_2O_3 as an adsorbent for oxy-anions of selenium has been demonstrated in batch systems to be more effective than DD-6 or activated γ-Al_2O_3, especially at low concentrations, it has not been soundly demonstrated in a packed bed system. In the future, tests with La_2O_3 should be conducted in plug flow with larger, non-soluble mixed oxide particles to prevent channeling and a large pressure drop. In this manner, the loading of the mixed oxide may be found and its performance at removing low concentrations of selenium optimized by altering the mass percent of La_2O_3.

Another area for improvement is in the processing methodology. For instance, previous workers have shown that 0.1 N sulfuric acid may be used to elute selenium from DD-6 with greater than 90% recovery. If the wastewater stream being remedied contains heavy metals, then the sulfuric acid may be the best possible elution reagent because sulfate ions will undergo ion exchange with oxy-anions of selenium, and hydrogen ions will undergo ion exchange with heavy metals cations, leaving the surface acidified as well. Hence, elution and activation may be accomplished with one reagent. In any processing scheme, flowrates and concentrations must also be optimized.

Although the packed bed model is based on the same fundamental equations as the batch model and produced reasonably good agreement with the experimental data, it is not amenable to predicting concentration profiles (breakthrough) at other bed lengths, solids concentrations, flowrates and so on. A more accurate solution to equations (73) and (74) may lead to better agreement between the experimental data and the model, and

enable the effect of volume as well as bed height to be accounted for. With modifications to the mass transfer coefficient for the ionic size gradient (to account for the decrease in dielectric constant between the bulk solution and the oxide-water interface), combined with a more accurate solution, the packed bed model can be made fully predictive in a manner similar to the batch model. However, both the batch and packed bed models will need to be validated by a more statistically sound set of experiments before being used. A rigorous model will be useful for optimizing flowrates, and designing, controlling, and estimating costs of packed bed wastewater treatment systems for removing oxy-anions of selenium.

XI. References:

1. Patterson, J.W., Industrial Wastewater Treatment Technology, Second Edition, Butterworths, Boston, 1985.
2. Williams, W.J., Handbook of Anion Determination, Butterworths, London, 1979.
3. Ramana, A., and Sengupta A.K., J. of Environmental Engineering, Vol. 118, No. 5, (1992).
4. Misra, M. Private communication.
5. EPA 440/5-80-070.
6. Hedrick, J.B., 1993 Annual Report. Rare Earths: The Lanthanides, Yttrium, and Scandium, U.S. Department of the Interior Bureau of Mines, March 1995.
7. MSDS for Lanthanum Oxide, obtained from ProChem, Inc., Rockford, IL 61109, 1994.
8. EPA 600/1-80-153.
9. MSDS for F-200, Activated γ-Al_2O_3, obtained from ADCOA, Gardena, CA 90247, 1994.
10. 40 CFR 141.11, 141.51, 141.62, 268.42, 268.43.
11. Harry M. Freeman, Standard Handbook of Hazardous Waste Treatment & Disposal, McGraw-Hill, Inc., New York, 1989.
12. Nayak, D.C., "Adsorption of Oxy-Anions of Selenium and Arsenic at Oxide/Water Interfaces." M.S. Thesis, University of Nevada, Reno, 1994.
13. Yang, K, Private communication.
14. Baes, C.F. Jr., and Mesmer, R.E., The Hydrolysis of Cations, Wiley-Interscience, New York, 1976.
15. Hunter, R.J., Zeta Potential in Colloid Science: Principles and Applications, Academic Press, London, 1981.
16. Davis, J.A., and Leckie, J.O., J. Colloid Interface Sci. Vol. 74, No. 1 (1980).
17. Hart, L.D., Alumina Chemicals Science and Technology Handbook, the American Ceramic Society, Inc., Westerville, Ohio, 1990.
18. Manceau, A. and Charlet, L., J. of Colloid Interface Sci. **168**, 87-93 (1994).
19. Davis, J.A., James, R.O., and Leckie, J.O., J. Colloid Interface Sci. Vol. 63, No. 3, (1978).
20. James, R.O., and Healy, T.W., J. Colloid Interface Sci. **40**, 65 (1972).
21. Weber, W.J., Physicochemical Processes for Water Quality Control. Wiley-Interscience, New York, 1972.
22. Marchant, W.N., "Method for Removing Soluble Selenium from Acidic Wastewater," U.S. Patent No. 3,933,635, 1976.
23. Baldwin, R.A., Stauter, J.C., and Terrell, D.L., "Process for Removal of Selenium from Aqueous Systems," U.S. Patent No. 4,405,464, 1983.
24. Baldwin, R.A., Stauter, J.C., Kauffman, J.W., and Laughlin, W.C., "Removal and Recovery of Selenium from Aqueous Solutions," U.S. Patent No. 4,519,913, 1985.

25. Fitzgerald, N.M., Richardson, J.H., Weaver, M.L., "Novel Magnesium Oxide-Aluminum Oxide (Hydrotalcite-like) Adsorbent for the Removal of Toxic Metals from Aqueous Streams," ALCOA Technical Center, Chemical Systems Division, ALCOA Center, PA 15069, 1992.
26. Adutwum, K.O., "Mechanism of Adsorption of Oxy-Anions of Selenium Onto Lanthanum Oxide and Alumina Oxide-Water Interfaces," M.S. Thesis, University of Nevada, Reno, 1995.
27. Islam, M.S., and Ilett, D.J., J. Phys. Chem. **98**, 9637 (1994).
28. Dufour, L.C., and Nowotny, J., Materials Science Forum, External and Internal Surfaces in Metal Oxides, Trans Tech Publications LTD, Switzerland, Vol. 29, 1988.
29. Hohl, H., and Stumm, W., J. Colloid Interface Sci. **55**, 281 (1976).
30. Peri, J.B., J. Phys. Chem. **69**, 211 (1965).
31. Peri, J.B., J. Phys. Chem. **69**, 220 (1965).
32. Regazoni, A.E., Blesa, M.A., and Marato, A.J.G., J. Colloid Interface Sci. **91**, 560 (1983).
33. Davis, J.A. and Leckie, J.O., J. Colloid Interface Sci. **67**, 90 (1976).
34. Atkins, P.W., Physical Chemistry, Fourth Edition, W.H. Freeman and Company, New York, 1990.
35. Bird, B.R., Stewart, W.E., and Lightfoot, E.N., Transport Phenomena, John Wiley & Sons, New York, 1960.
36. Adamson, A.W., Physical Chemistry of Surfaces. John Wiley and Sons, Inc., New York, 1990.
37. Moya, A.A., Castilla, J., and Horno, J., J. Phys. Chem. **99**, 1292 (1995).
38. McCabe, W.L., Smith, J.C., and Harriot, P., Unit Operations of Chemical Engineering, Fifth Edition, McGraw-Hill, Inc., New York, 1993.
39. Felder, R.M., and Rousseau, R.W., Elementary Principles of Chemical Processes, Second Edition, John Wiley & Sons, New York, 1986.
40. Peters, M.S., and Timmerhaus, K.D., Plant Design and Economics for Chemical Engineers, Fourth Edition, McGraw-Hill, Inc., New York, 1991.
41. Krestov, G.A., Thermodynamics of Solvation: Solution and Dissolution; Ions and Solvents: Structure and Energetics, Ellis Horwood, New York, 1991.
42. Horvath, A.L., Handbook of Aqueous Electrolyte Solutions: Physical Properties, Estimation and Correlation Methods, John Wiley & Sons, New York, 1985.
43. Harris, D.C., Quantitative Chemical Analysis, 3rd Ed., W.H. Freeman & Company, New York, 1992.
44. Van Dyke, M., Private communication.
45. Murphy, A.P., Ind. Eng. Chem. Res. **27**, 187 (1988).

XII. Appendix:

i. Acknowledgments:

The author wishes to acknowledge the financial support provided by the USBM, Generic Center for Waste Treatment and Recovery (Grant # G1145232), and ENCYCLE/Texas. Ms. Cathy F. Neve, Process Engineer, ENCYCLE/Texas, analyzed samples from the packed bed tests with their ICP, as well as provided wastewater samples from their treatment facility in Corpus Christie, Texas. Her support was greatly appreciated. Further thanks are extended toward the undergraduate Chemical Engineering students who assisted with operating and running the packed beds, and helped develop and construct the data acquisition and control system. Finally, my advisor and closest peer, Dr. Manoranjan Misra, was a great help in planning experiments, interpreting results, and correcting papers for publication.

ii. Nomenclature:

ρ	Liquid density, kg/m^3
$\Delta G_{ads,j}$	Free energy of adsorption for an ionic species, J/mole.
$\Delta G_{chem,j}$	Free energy due to chemical interaction of ion with surface, J/mole
$\Delta G_{coul,j}$	Free energy from coulombic attraction of ion with charged surface, J/mole
$\Delta G_{ds,j}$	Free energy due to ion losing part of its hydration sheath, J/mole
α_j	Fraction remaining of an ionic species
Γ_j	Surface excess, mg/m^2
ε_o	Permitivitty in a vacum, $C^2/J\text{-}m$
ε_r	The internal dielectric constant
ε	External void fraction of packed bed
Φ	Function
ζ	Zeta potential, mV
ψ, ψ_o	Electrostic potential or surface potential, Volts
ρ_B	Bulk density of oxide in packed bed, kg/m^3
δ_j	Boundary layer thickness for an ion, m
ν_j	Molar ionic conductivity of a species, $C^2\text{-}m^2/J\text{-}s\text{-}mole$; or a model constant
τ_j	Time constant for adsorption of a species, s
$\alpha_{j,ss}$	Fraction remaining of a species as time approaches infinity
$\psi_{o,ss}$	Initial surface potential of adsorbent, Volts

A	Cross sectional area of packed bed, cm^2
A_{sp}	Specific surface area of solid, m^2/g of solid
C_j	Bulk concentration, ppm
$C_{j,ss}$	Initial bulk concentration of an ionic species in the packed bed, ppm
$C_{o,j}$	Initial bulk concentration or inlet concentration to packed bed, ppm
C_s	Solids concentration, kg of solid/m^3 of solution
$C_{s,j}$	Concentration of an ion on the oxide surface, ppm
D_j	Diffusion coefficient of an ionic species, m^2/s
D_p	Mass or geometric average particle diameter, m
e	Charge of an electron, C
E	Electric field strength, volt/m, or half cell potential, V
F	Faraday's constant, 96,485 C/mole
$F_{ds,j}$	Molar force of desolvation of an ion, N/mol
f_j	Ionic friction factor, Kg/m-s-ion
$F_{j,}$	Force due to an electric field, N/mole
F_j	Frictional force, N/mole
h,h_{ss}	Height or steady state height of liquid in packed column, m
h_{solid}	Height of solid in packed column, m
I	Ionic strength, mol/liter
$J_{ads,j}$	Total ionic adsorption flux of a species,mg/s-m^2
$J_{coul,j}$	Flux due to coulombic attraction or repulsion of an ion, mg/m^2-s
$J_{diff,j}$	Flux due to diffusion of an ion, mg/m^2-s
$J_{ds,j}$	Flux due to desolvation of an ion, mg/m^2-s
k	Second-order rate constant, 1/ppm-s
k_j,k_{aj}	Mass transfer coefficients, nm/s
L	Bed length, m
$LA^{(T)}$	Mixture of 10% La_2O_3 and 90% activated transition (γ) Al_2O_3
N_A	Avagadro's constant, atoms/molecule
N_{Re}	Reynolds number
pH_o	Initial pH of bulk solution
pH_{zpc}	pH at which the zero point of charge occurs
q_o,q_i	Output and input volumetric flowrate for packed bed, ml/min
R	Universal gas constant, 8.314 J/mole-°K
$r_{H,j},r_{e,j}$	Hydration or effective radius of an ionic species, nm
rpm	Revolutions per minute, rev/min
s	Laplace domain variable for time, 1/liters
s_j	Drift speed of an ion, m/s
T	Temperature, °K
t	time, s
u	Viscosity of solution, kg/m-s
V	Total volume treated from first entry to column, liters
V_L	Total volume treated compensated for total dead volume, liters
V_o	Velocity or volume treated, m/s or liters